



Research paper

Antitumor agents 7. Synthesis, antiproliferative activity and molecular modeling of new L-lysine-conjugated pyridophenoxazinones as potent DNA-binding ligands and topoisomerase II α inhibitors

Silvana Pedatella^a, Carmen Cerchia^b, Michele Manfra^{c, **}, Anna Cioce^d, Adele Bolognese^a, Antonio Lavecchia^{b, *}

^a Department of Chemical Sciences, University of Naples Federico II, via Cynthia 6, Monte Sant'Angelo, 80126, Naples, Italy

^b Department of Pharmacy, "Drug Discovery" Laboratory, University of Naples Federico II, via D. Montesano 49, 80131, Naples, Italy

^c Department of Science, University of Basilicata, viale dell'Ateneo Lucano 10, 85100, Potenza, Italy

^d Department of Glycotechnology, CIC biomaGUNE, Paseo Miramón 182, 20009, San Sebastián, Spain

ARTICLE INFO

Article history:

Received 16 September 2019

Received in revised form

20 November 2019

Accepted 9 December 2019

Available online 14 December 2019

Keywords:

Pyridophenoxazinones

Antiproliferative activity

DNA damage

Topoisomerase II inhibitors

Docking studies

ABSTRACT

A series of L-lysine-conjugated pyridophenoxazinones **2–5** and **2'–5'** were designed and synthesized for developing compounds with multimodal anticancer potentialities. All compounds inhibited the proliferation of a panel of human liquid and solid neoplastic cell lines. **2** and **5** were the most active compounds with IC₅₀ values in the submicromolar range. UV–vis, ¹H NMR, unwinding, and docking experiments demonstrated that they intercalate between the middle 5'-GC-3' base pairs with the carboxamide side chain lying into major groove. Charge-transfer contribution to the complex stability, evaluated by *ab initio* calculations, was found to correlate with cytotoxicity. Relaxation and cleavage assays showed that **2** and **5** selectively target Topo II α over Topo II β and stimulate the formation of covalent Topo II–DNA complexes, functioning as poisons. Moreover, compound **5** induced DNA damage and arrested MCF-7 cells at the G2/M phase. Altogether, the work provides interesting structure-activity relationships in the pyridophenoxazinone-L-lysine conjugate series and identifies **5** as a promising candidate for further in vivo evaluation.

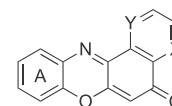
© 2019 Elsevier Masson SAS. All rights reserved.

1. Introduction

DNA represents one of the most investigated targets for cancer treatment. A wide variety of chemotherapeutic drugs belong to the class of DNA-intercalating agents [1]. Intercalators typically bind to DNA by inserting a planar aromatic chromophore between adjacent base pairs, inducing substantial changes in DNA structure and causing unwinding of the DNA helix. As such, chemotherapeutic intercalators inhibit DNA replication in rapidly growing cancer cells.

PPH-I and PPH-II are 5H-pyridophenoxazin-5-one derivatives endowed with high cytotoxic properties on several lymphoblastoid

and solid tumor cell lines [2–4]. Molecular modeling calculations and ¹H NMR investigations suggested that the pyridophenoxazinone skeleton binds to DNA through an intercalation mode by π – π stacking and electrostatic interactions with the DNA base pairs [2–4]. Furthermore, pyridophenoxazinones can engender free radical intermediates leading to oxidative-stress-induced cell death [5]. Therefore, PPH-I and PPH-II possess multimodal cytotoxic activity including DNA intercalation, metal-chelating ability and radical production aptitude.



PPH-I X = N; Y = CH
PPH-II X = CH; Y = N

Several DNA-intercalating agents are also able to affect topoisomerase catalytic activity, thus producing permanent DNA strand

* Corresponding author. Department of Pharmacy, "Drug Discovery" Laboratory, University of Naples Federico II, 80131, Naples, Italy.

** Corresponding Author. Department of Science, University of Basilicata, viale dell'Ateneo Lucano 10, 85100, Potenza, Italy.

E-mail addresses: michele.manfra@unibas.it (M. Manfra), antonio.lavecchia@unina.it (A. Lavecchia).

Abbreviations			
ACHN	human renal adenocarcinoma	HT-29	human colon adenocarcinoma
AMD	actinomycin D	LMP2	local Møller-Plesset second-order perturbation theory
AMSA	amsacrine	MCF-7	human breast adenocarcinoma
ATCC	American type Culture Collection	MT-4	humanCD4+ T cell expressing the TATA gene of leukemia
BSA	bovine serum albumin	MTT	3-(4,5-dimethylthiazol-2-yl)-2,5-diphenyltetrazolium bromide
BSSE	basis set superposition error	MW	microwave
CCRF-CEM	human acute T-lymphoblastic leukemia	NBO	natural bond orbital
CCRF-SB	human acute B-lymphoblastic leukemia; Comet assay, single cell gel electrophoresis	PBS	phosphate buffered saline
ctDNA	calf thymus DNA	RIPA	(radio-immunoprecipitation assay)
Doxo	doxorubicin	PMSF	(phenylmethylsulfonyl fluoride)
DTT	dithiothreitol	PVDF	poly(vinylidene fluoride)
EDC	1-ethyl-3-[3-dimethylaminopropyl]carbodiimide hydrochloride	RPMI	Roswell Park Memorial Institute
EIMS	electronic ionization mass spectra	SDS	sodium dodecyl sulfate
EtBr	ethidium bromide	SKMEL-28	G-361, human skin melanoma
FCS	fetal calf serum	TAE	Tris-acetate-EDTA
H-bonds	hydrogen bonds	THF	tetrahydrofuran
HeLa	cervix carcinoma	TLC	thin-layer chromatography; Topo, topoisomerase
HOBT	hydroxybenzotriazole	VP-16	etoposide.

breaks [1,6–8]. Topoisomerases are enzymes responsible for coordinating DNA topology by catalyzing DNA cleavage and re-ligation. Thus, the ability to interfere with these enzymes or generate enzyme-mediated damage is an effective strategy for cancer therapy [9,10]. Depending on their mechanism, topoisomerases are classified in two main groups: type I topoisomerase (Topo I) and type II topoisomerase (Topo II). Topo I cleaves one strand of a DNA double helix to be relaxed and then rejoined. Topo II cleaves both strands of one DNA duplex to make another non-cleaved duplex pass through a transient, Topo II-mediated break and then followed by reannealing the cleaved strands. Human Topo II is categorized into two subclasses, namely, Topo II α and Topo II β . Topo II α is a cell cycle dependent enzyme; it peaks during G2/M phase and decreases at the end of mitosis. The overexpression of Topo II α is only observed in proliferating cells, but the expression of Topo II β is not changed during the cell cycle. The majority of Topo poisons are cytotoxic via stabilization of the normally transient, covalently bound cleavable complex formed between DNA and enzyme. Drug stabilized DNA-enzyme complexes (ternary complexes) are believed to be lethal upon DNA replication when irreversible double-stranded DNA breaks are formed, causing various chromosomal aberrations culminating in cell death [11,12].

The inhibition of Topo II α , rather than Topo II β , has been reported as a well-defined approach to develop novel antineoplastic agents because Topo II α is necessary for the hypercompaction of mitotic chromosomes in human cells, whereas inhibitors targeting Topo II β have been frequently associated with undesirable side effects, such as drug resistance, cardiotoxicity, or secondary malignancies [13,14]. The development of resistance to Topo-targeting drugs, however, presents a major clinical problem; resistance commonly is manifested as classical multidrug resistance, which leads to increased efflux of drug from the cell, thereby reducing cytotoxic efficacy [15] and clinical applications. For these reasons, medicinal chemistry research efforts have been recently devoted to the development of new Topo II α -specific inhibitors as anticancer agents [7,16–22].

In the present study, we postulated that combining a tetracyclic

planar chromophore with a flexible cationic side chain capable of more than one DNA groove or Topo interaction could modulate the DNA-binding properties and consequently the pattern of Topo enzyme inhibition. It was indeed recognized that a basic chain, protonated a physiological pH of 7.4, would be expected to produce strong electrostatic interactions with the negatively charged phosphate groups on DNA skeleton, reinforcing the affinity of the compound for DNA. Also, the attachment of an amino acid or a peptide to an intercalating drug could effectively increase its selectivity against tumor cells [23]. For example, conjugates of doxorubicin (Doxo), daunorubicin, and mitoxantrone with an amino acid or peptides show more selective antitumor activity than the drugs themselves [24–33]. Finally, the attachment of an amino acid or a peptide to the drug could also increase its solubility in aqueous solutions, overcoming administration problems as well as multidrug resistance protein-mediated drug efflux and toxicity [34,35]. Typical examples of this class of substituted intercalators are amonafide [36], TAS-103 (BMS-247615) [37,38], DACA [39] and S-16020 [40] (Fig. 1). Based on this rationale, a new series of 5H-pyrido[3,2-a]phenoxazin-5-one (**2–5**) and 5H-pyrido[3,2-a]phenoxazin-5-one (**2'-5'**) carboxamides (Fig. 1) bearing a flexible basic L-lysine side chain at position 9 and 10 of ring A of the pyridophenoxazinone framework was synthesized. The N-terminal α -amino or ϵ -amino group of L-lysine was linked to chromophore via an amide linkage.

Here, we report the synthesis of new PPHI- and PPHII-L-lysine-conjugates (**2-5**- and **2'-5'**) together with a first evaluation of their biological activities. The DNA binding characteristics of these molecules were examined using a range of biochemical and biophysical methods, and their effects on cytotoxic power, Topo I and II inhibitory activity and the cell cycle progression were investigated. The structure of **2–5** complexed with the d(GAAGCTTC)₂ octamer was analyzed by ¹H NMR and supported by docking studies. Moreover, *ab initio* calculations were carried out on the model “sandwich” complexes of L-lysine-conjugated pyridophenoxazinones with flanking DNA base pairs to establish how the π - π stacking interactions affect the binding of compounds to DNA.

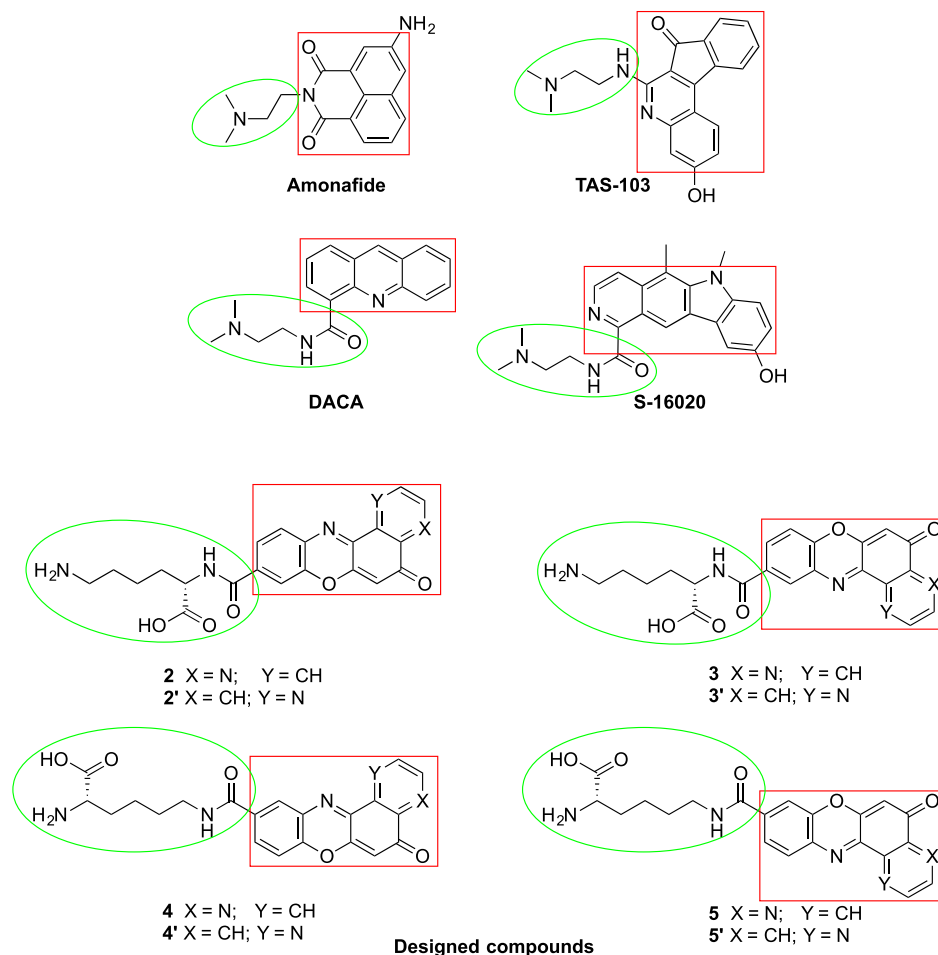


Fig. 1. PPH-I, PPH-II, selected DNA-intercalating agents and our designed L-lysine-conjugated pyridophenoxazinones **2–5** and **2'–5'**.

2. Results and discussion

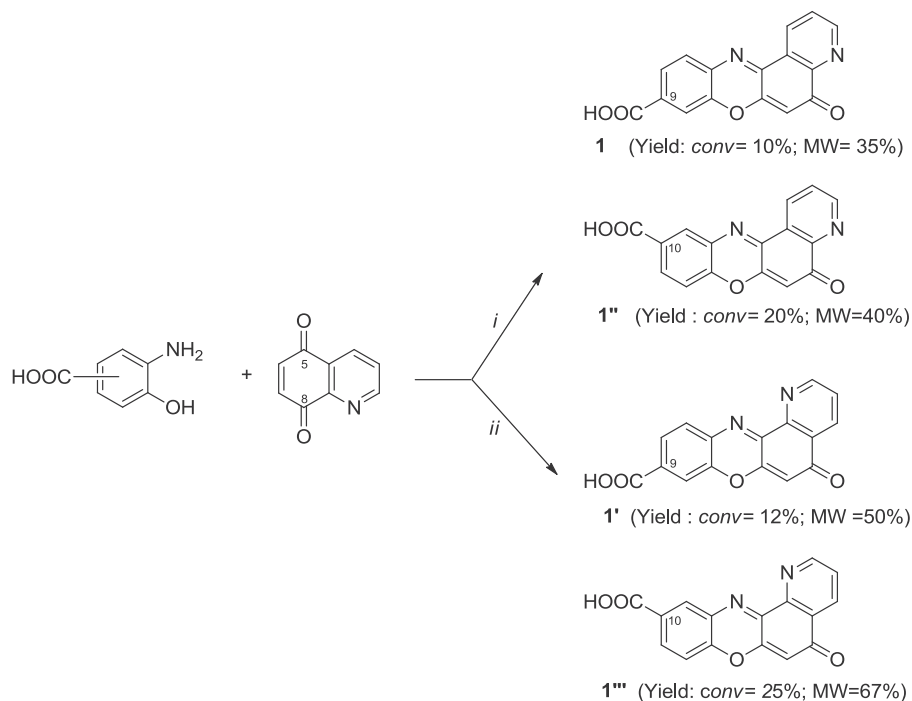
2.1. Chemistry

The synthetic procedure to prepare **2–5** and **2'–5'** required three main steps: i) preparation of pyridophenoxazinone carboxylic acids **1–1'** and **1''–1'''**, ii) preparation of differently masked L-lysines on the α -, ϵ -amino and carboxy groups, and iii) coupling reaction between the carboxylic acids **1–1'** and **1''–1'''** and differently protected L-lysines. Scheme 1 reports the reactions between equimolecular amounts of 3-amino-4-hydroxybenzoic acid or 3-hydroxy-4-amino-benzoic acid and the quinoline-5,8-dione, in acetic acid at refluxing temperature, which gave rise to **1–1'** and **1''–1'''**, respectively. This conventional procedure (*conv*) was described to prepare similar compounds in our previous papers (Scheme 1) [2,4].

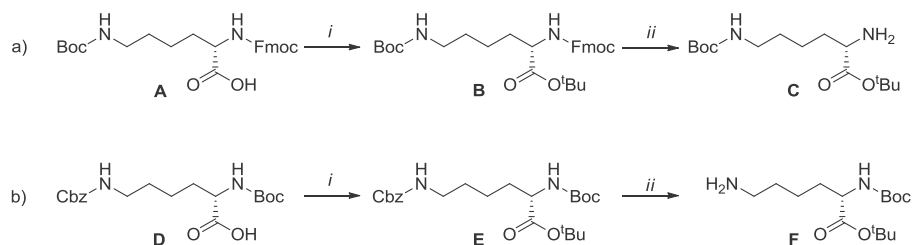
The conventional procedure was very expensive and required long reaction times, and furnished very poor yields. Several side products, like phenoxazines, aminophenoxazin-3-ones, triphenodioxazines accompanied the desired pyridophenoxazinone acids. These by-products together with black, intractable, polymeric materials decreased significantly the yields of the expected acids and encumbered the subsequent purification procedures. It is reasonable to assume that the presence of the withdrawing carboxy group in *para* position to the amino group of the *ortho* amino phenol decreases its reactivity and minimizes the reaction yields. The smaller detrimental effects, observed when the carboxy group lies in *para* position to the phenol hydroxyl group, suggests the

hypothesis that the amino group firstly attacks the quinoline-5,8-dione [2]. Under these circumstances, we considered worthwhile to employ a microwave (MW) assisted synthetic procedure to obtain **1–1'** and **1''–1'''** with better yields, very short reaction times and, more importantly, with diminished production of black polymeric residues. Therefore, the reaction was performed in a MW CEM Discover apparatus at 50 W for 30' of continuous irradiation, and was found to yield better results. Compounds **1–1'** and **1''–1'''** were recovered from the reaction mixture with a yield of 30–65% and this result seemed to suggest that a dehydration Step, promoted by MW heating, could play a crucial role in the mechanism of this reaction. Scheme 1 reports the yields obtained using the *conv* and MW procedures.

The second reaction Step consisted in preparation of differently masked L-lysines on the α -, ϵ -amino and carboxy groups to use in the successive copulation reaction with the acids **1–1'** and **1''–1'''**. Scheme 2 details the synthetic procedures used starting from the commercial Fmoc-L-lys(Boc)OH (**A**) and Boc-L-lys(Cbz)OH (**D**), respectively. **A** was esterified at the carboxy group in dry dichloromethane with *tert*-butyl 2,2,2-trichloroacetimidate in presence of boron trifluoride diethyl etherate to form the corresponding butyl ester **B**, which furnished the α -amino L-lysine *tert*-butyl ester **C** by treatment with piperidine in acetonitrile (Scheme 2a). To gain access to the ϵ -amino function, **D** was used and converted into intermediate (**E**). After esterification, the ϵ -amino group of **E** was de-protected yielding **F** by a reduction reaction with Palladium/Carbon in methanol (Scheme 2b).



Scheme 1. Synthetic route of compounds **1-1'** and **1''-1'''**. Reagents and conditions: *i.* 3-amino-4-hydroxybenzoic acid or 3-hydroxy-4-amino-benzoic acid, quinoline-5,8-dione, Co(II) acetate, CH₃COOH, MW assisted heating 15', 50 W; *ii.* 3-amino-4-hydroxybenzoic acid or 3-hydroxy-4-amino-benzoic acid, quinoline-5,8-dione MW assisted heating 15', 50 W.



Scheme 2. Synthetic route of compound **C** and **F**. Reagents and conditions: a) *i.* *t*-Butyl-2,2,2-trichloroacetamidate, boron trifluoride diethyl etherate, CH₂Cl₂ dry, rt, overnight; *ii.* Piperidine, CH₃CN, 0 °C → rt, 3.5 h. b) *i.* *t*-Butyl-2,2,2-trichloroacetamidate, boron trifluoride diethyl etherate, CH₂Cl₂ dry, rt, overnight; *ii.* H₂, 5% Pd/C, MeOH, rt, 3.5 h.

In the third reaction Step, the ϵ - and α -protected Boc-L-lysine *t*-butyl esters, **C** and **F**, were used in the coupling reactions with the pyridophenoxazinone acids **1-1'** and **1''-1'''** to form the designed carboxamides. **Scheme 3** details the overall synthetic procedure of the formation of **2-5** and **2'-5'**.

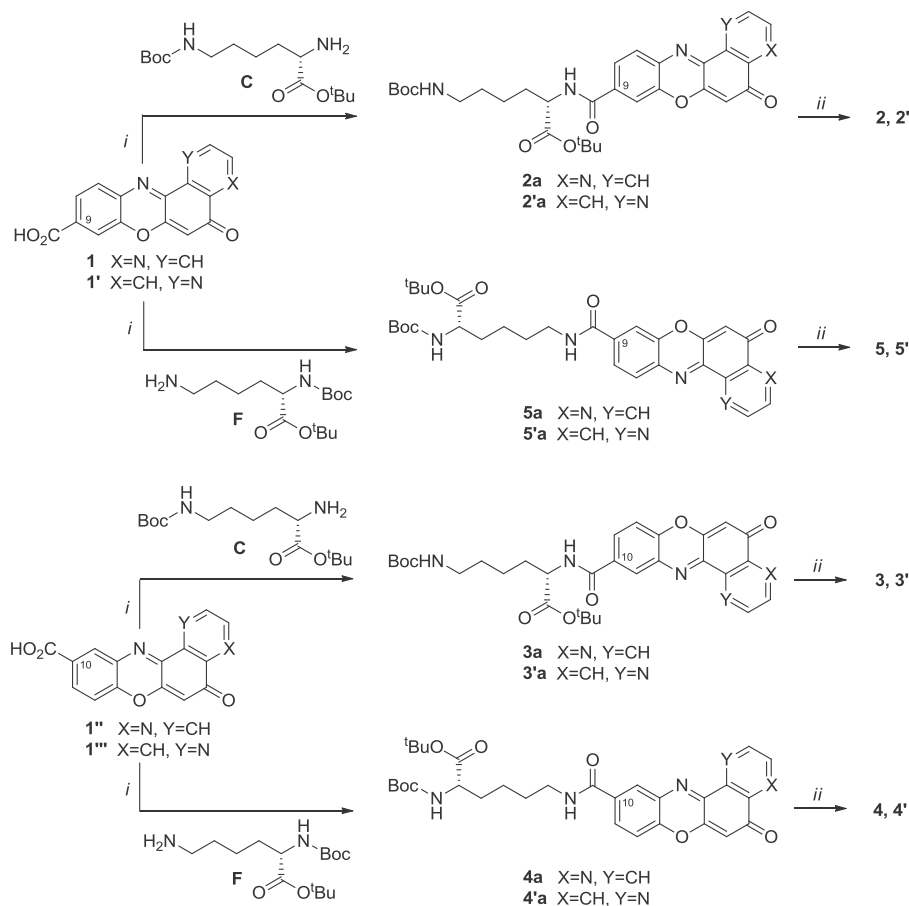
To the anhydrous solutions of phenoxazinones **1-1'** and **1''-1'''**, dissolved in THF at 0 °C, an equimolar quantity of hydroxybenzotriazole (HOBt) was added to activate the carboxy group. After 30 min, equimolar quantities of masked suitable L-lysine **C** or **F** and of 1-ethyl-3-[3-dimethylaminopropyl]carbodiimide hydrochloride (EDC) in anhydrous tetrahydrofuran (THF) were added to the reaction mixtures. The solutions were stirred at 0 °C for 1 h and then allowed to warm slowly to room temperature. After 12 h, the solvent was evaporated and the crude products, containing the appropriate, masked carboxamides, were dissolved in AcOEt and washed with saturated aqueous solution of NH₄Cl. The crude products **2a-5a** and **2'a-5'a** were de-protected with formic acid at room temperature yielding **2-5** and **2'-5'** (**Scheme 3**). Further purification was performed with thin-layer chromatography (TLC) on silica gel plates using chloroform-methanol (80:20; v:v, as eluent). ¹H NMR spectra of starting phenoxazinones **1**, **1'**, **1''** and **1'''** are included as Supplementary data (**Figs. S1-S4**) together with ¹H

NMR spectra and HPLC data of the final compounds **2-5** and **2'-5'** (**Figs. S5-S12**).

2.2. Antiproliferative activity

The antiproliferative activity of the L-lysine-conjugated pyridophenoxazinones **2-5** and **2'-5'** was evaluated against a panel of human cancer cell lines representative of liquid and solid tumors and the results are shown in **Table 1**. The activities, reported as IC₅₀ (μM) values, were compared with those of PPH-I, PPH-II from our laboratory and commercial Doxo, AMD, and etoposide (VP-16).

The tested compounds showed diverse activity against the liquid and solid tumor cells, being the last ones more sensitive to their antiproliferative effect. Only **5** showed comparable activity on both solid and liquid cancer cells. The IC₅₀ values of derivatives **2-5** were lower than the corresponding IC₅₀ reported for derivatives **2'-5'**. Moreover, **2-5** showed a cytotoxic power on solid cell lines comparable to that of the reference compound AMD and higher than that of Doxo, VP-16 as well as PPH-I and PPH-II. The maximal potency was achieved with **2** and **5** bearing the L-lysine carboxamide side chain attached to the 9 position of pyridophenoxazinone system through α - and ϵ -amino group, respectively. The



Scheme 3. Synthetic route of compounds **2–5** and **2'-5'**. Reagents and conditions: *i*. HOBT, THF dry, 0 °C, 30'; *C* or *F*, EDC, 1 h 0 °C, 12 h at r.t.; *ii*. AcOEt/NH₄Cl; HCOOH, rt.

Table 1
Antiproliferative activity of compounds **2–5** and **2'-5'** on human liquid and solid cancer cell lines.

Cpd	IC ₅₀ (μM) ^a									
	CCRF-CEM	CCRF-SB	MT-4	HT-29	MCF-7	HeLa	ACHN	SKMEL-28	G-361	
2	0.02	0.02	0.01	0.003	0.007	0.005	0.008	0.002	0.001	
2'	0.017	0.08	0.20	0.10	0.05	0.05	0.06	0.06	0.05	
3	0.10	0.12	0.09	0.08	0.10	0.08	0.10	0.12	0.06	
3'	0.16	0.16	0.20	0.20	0.10	0.10	0.08	0.21	0.05	
4	0.04	0.08	0.09	0.02	0.06	0.05	0.05	0.04	0.02	
4'	0.15	0.10	0.15	0.12	0.12	0.15	0.10	0.10	0.03	
5	0.003	0.005	0.006	0.004	0.003	0.005	0.005	0.002	0.006	
5'	0.15	0.16	0.20	0.10	0.12	0.10	0.07	0.08	0.09	
PPH-I	0.01	0.01	0.01	0.25	0.23	0.20	0.01	0.21	0.01	
PPH-II	0.09	0.15	0.18	0.38	0.37	0.15	0.23	0.40	0.45	
Doxo ^b	0.02	0.03	0.01	0.15	0.05	0.20	0.04	0.06	0.09	
AMD ^b	0.001	0.002	0.001	0.006	0.006	0.008	0.005	0.002	0.006	
VP-16 ^b	1.20	0.10	1.25	2.50	1.00	3.00	2.15	1.10	2.30	

^a Compound concentration required to reduce cell proliferation by 50%, as determined with the MTT method, under conditions allowing untreated controls to undergo at least three consecutive rounds of multiplication. Data represent mean values for three independent determinations. CCRF-CEM, human acute T-lymphoblastic leukemia; CCRF-SB, human acute B-lymphoblastic leukemia; MT-4, humanCD4+ T cell expressing the TATA gene of leukemia; HT-29, human colon adenocarcinoma; MCF-7, human breast adenocarcinoma; HeLa, cervix carcinoma; ACHN, human renal adenocarcinoma; SKMEL-28, G-361, human skin melanoma.

^b Controls.

most sensitive cells to the cytotoxic effect of **2** and **5** were HT-29 (IC₅₀ of 0.003 and 0.004 μM), SKMEL-28 (IC₅₀ of 0.002 and 0.002 μM), MCF-7 (IC₅₀ of 0.007 and 0.003 μM) and G-361 (IC₅₀ of 0.001 and 0.006 μM). It is interesting that the antiproliferative activity of the two series of L-lysine-conjugates, **2–5** and **2'-5'**, was generally higher than the activity of the parent unsubstituted compounds PPH-I and PPH-II. The difference of activity between

the two series **2–5** and **2'-5'** probably results from their different mechanisms of action and suggests that the position of pyridine nitrogen within the pyridophenoxazinone skeleton plays an important role in the antiproliferative activity of the tested compounds. Moreover, the position of L-lysine side chain on the pyridophenoxazinone ring, as well as the α- or ε-amino group involved in the amide bond formation affect the difference in the cytotoxic

activity between the two series **2–5** and **2'-5'** and within each series. To better highlight the mechanism of action of the pyridophenoxazinone ι -lysine-conjugates, their DNA binding properties and Topo I and II inhibition were investigated.

2.3. DNA binding properties

Compounds **2–5** and **2'-5'** were tested to assess whether they interacted with DNA. The interaction of ι -lysine-conjugates with calf thymus DNA (ctDNA) was monitored by optical spectrophotometric titrations in phosphate buffer, pH 7. The UV–Vis spectra of compounds showed a significant absorption in the range of 430–469 nm, typical for transitions between π -electron energy levels. When DNA binding occurs, the compounds are inserted in a different environment than the uncomplexed form in solution, which promote the distortion of the electron distribution upon π -stacking with the bases. This accounts for the significantly different compound absorption features in the complexed and uncomplexed forms [41]. The spectroscopic properties of **2–5** and **2'-5'** in the presence and absence of ctDNA showed hypochromism and red shift due to the formation of stable DNA-ligand complexes, suggesting that they act as DNA intercalating compounds. The presence of isosbestic points suggested that the compounds present a single DNA binding mode. Table 2 lists the spectroscopic data of the ι -lysine-conjugates in the absence and in presence of ctDNA.

2.4. UV–visible spectroscopic analysis of 5-DNA complexes

Fig. 2A shows the absorption spectra of free ctDNA and its complexes with varying concentration of compound **5**, chosen as representative of series **2–5**. When **5** interacts with DNA, it causes hyperchromic effect (increase in absorbance of DNA) with increasing concentration of **5** in solution. This phenomenon is coupled with the 10 nm shift in the absorbance maxima from 260 nm to 250 nm (hypsochromic or blue shift). Increase in absorbance along with the hypsochromic shift is attributed to the intercalation of the chromophore of **5** between the DNA base pair.

The binding constant (K) represents a quantitative measurement of binding of **5** with DNA. In this work, K has been determined by using the “mole ratio method”, which involves the preparation of multiple solutions of drug–DNA complex, keeping the concentration of DNA constant while varying the drug concentration from 1×10^{-1} mM to 3×10^{-2} mM. It is evaluated by examining the variations in the optical density at 260 nm for free DNA (represented by A_0) and its complexes with **5** (represented by A) [42,43]. Since the double reciprocal plot of $1/(A - A_0)$ vs. $1/(\text{drug concentration})$ is linear, K can be calculated from the ratio of the intercept to the slope [43–48] (Fig. 2B). The binding constant for this interaction is $3.8 \times 10^5 \text{ M}^{-1}$, which demonstrates the high affinity of **5** for DNA double helix. The value of binding constant obtained is consistent with those reported for the interaction of anthracycline molecules with DNA [48–51].

Table 2
Isosbestic point (nm), λ_{max} , and % of hypochromic effect of compounds **2–5** and **2'-5'**.

	2	2'	3	3'	4	4'	5	5'
λ_{max}	443	451	437	445	436	441	443	459
ϵ	5736	5928	5316	8431	6620	1792	4219	1216
Isosbestic point	395	297	343	280	310	275	340	320
Red shift	447	455	440	447	440	446	448	461
% hypochromism	28	26	30	19	39	17	58	17

2.5. Unwinding assay

The most powerful cytotoxic compounds of series **2–5** were investigated through unwinding assays and ^1H NMR spectroscopic experiments using the double strand octamer $[\text{d}(\text{GAAGCTTC})]_2$, expressly synthesized to intercalate the pyridophenoxazinone chromophore [2]. The unwinding assay is based on the formation of constrained negative supercoils and compensatory unconstrained positive supercoils in covalently closed circular DNA by an intercalative agent. When an intercalated plasmid is treated with human Topo I, the unconstrained positive supercoils are removed. The extraction of the intercalative agent allows the redistribution of the constrained negative supercoils throughout the DNA molecule and the conversion of the relaxed DNA into negatively supercoiled DNA [52]. Thus, the DNA unwinding assay is designed to directly measure the extent of the drug-induced negative supercoils.

The DNA unwinding assay was performed using the relaxed plasmid pBR322 in the presence of various concentrations of the more active derivatives **2–5**. Ethidium bromide (EtBr) was used as control. All compounds significantly changed the topological state of plasmid pBR322 at 10 μM concentration (Fig. 3, lanes C, F, I and N, respectively), and **2** and **5** exhibited a more marked unwinding at the lowest 0.1 μM concentration (Fig. 3, lanes B and M, respectively). It should be noted that the cytotoxicity of the four compounds ($5 \approx 2 > 3 \approx 4$) correlated well with the levels of DNA negative supercoils induced by these compounds. A strand passage assay for human Topo I displayed that the ι -lysine-conjugates did not affect the catalytic activity of Topo I (data not shown).

2.6. ^1H NMR spectroscopic analysis

Quantitative titrations of the octamer $[\text{d}(\text{GAAGCTTC})]_2$ with compounds **2–5** were performed into a NMR tube of a 500 MHz spectrometer, at probe temperature of 25 $^\circ\text{C}$ where the proton signals can be resolved without compromising the octamer duplex stability. ^1H NMR spectra, before and after addition of pyridophenoxazinone- ι -lysine conjugates to $[\text{d}(\text{GAAGCTTC})]_2$ (2:1 M ratio), were executed in 99.99% D_2O 10 mM phosphate buffer, pH 7. In phosphate buffer the resonances of **2–5** all broadened significantly and characteristic changes were observed for both octamer and ligand protons. Table 3 shows the ^1H NMR resonance values of **2–5** and their complexes to $[\text{d}(\text{GAAGCTTC})]_2$. Fig. 4 illustrates the spectra of the compound **5**, the octamer, and the corresponding complex, taken as representative of the behavior of whole series. Spectra of compounds **2–4** are included as Supplementary data (Figs. S13–S15).

The spectral features of the ι -lysine derivative/octamer complexes showed that all the signals of the downfield pyridophenoxazinone moiety shifted to higher field in the area of the spectrum characteristic of the DNA base pairs resonances (7.74 and 7.48 δ). This shift indicates that the pyridophenoxazinone moiety is shielded by the magnetic field produced by ring currents due to the bases owing to the π - π stacking interactions typical of the intercalative binding of a planar polycyclic system into DNA double helix (Table 3 and Fig. 4). Moreover, the general chemical shift perturbation of non-exchangeable octamer protons respect to those of the unmodified palindromic duplex structure can be due also to lack of symmetry of the base sequences related to the presence of the ligand and to its interactions. The large shift of protons H_6 of **2–5** toward higher field in all the complexes (ranging between 0.38 and 0.10 ppm) seems to underline the different involvement of the electron-acceptor iminoquinone system in the π - π stacking interactions with DNA base pairs (Table 3). As regards the protons of lysine side chains, it is to note that upon complex formation, they are pushed toward lower field. The magnitude of these shifts can be

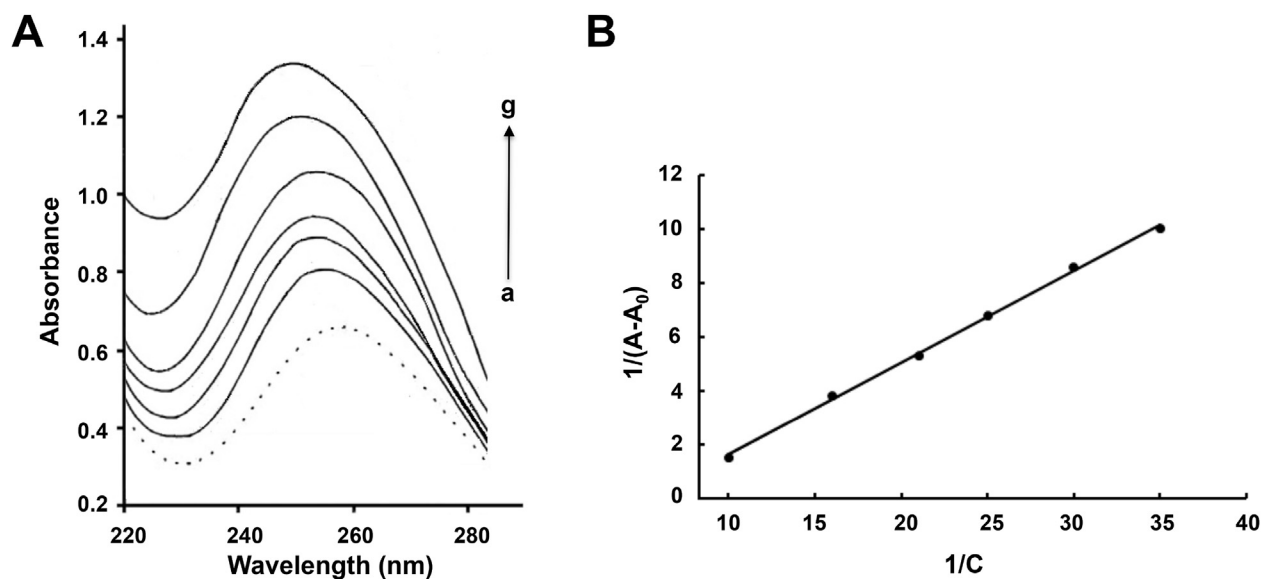


Fig. 2. (A) UV–Visible spectra of free calf thymus DNA (0.2 mM) in the absence and presence of **5** leading to drug: DNA ratio of (a) 0:1 (free calf thymus DNA) (b) 1:1 (c) 2:1 (d) 3:1 (e) 4:1 (f) 5:1 (g) 6:1. (B) Double reciprocal plot of **5** binding to DNA. A_0 is the initial absorption of free DNA and A is the absorption at different concentrations at 260 nm. C is the analytical concentration of **5** in solution.

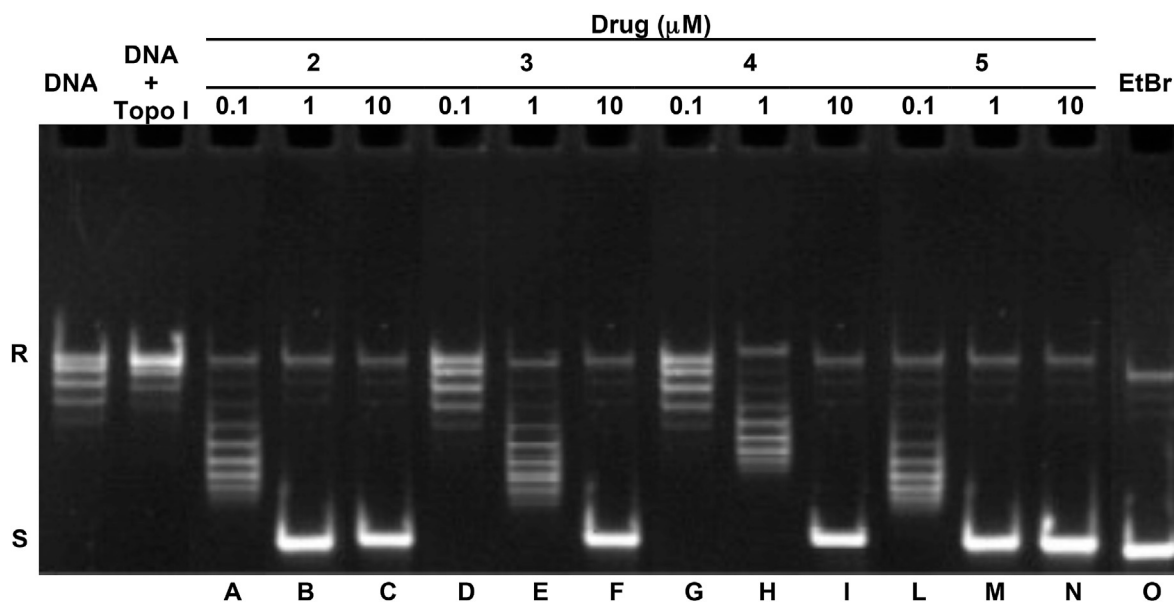


Fig. 3. L-Lysine-conjugates **2–5** intercalate into DNA. The DNA unwinding reaction mixtures contained 0.3 μg of relaxed plasmid pBR322 DNA, 2 units of human Topo I, and the indicated concentrations of the various compounds (lanes A–N). Three independent experiments for each assay exhibited essentially identical results; EtBr (2 μM) was used as control.

affected, at different extent, by ionic or H-bond interactions with both backbone and base pairs of octamer according to the relative positioning of the guest molecule into the intercalation site.

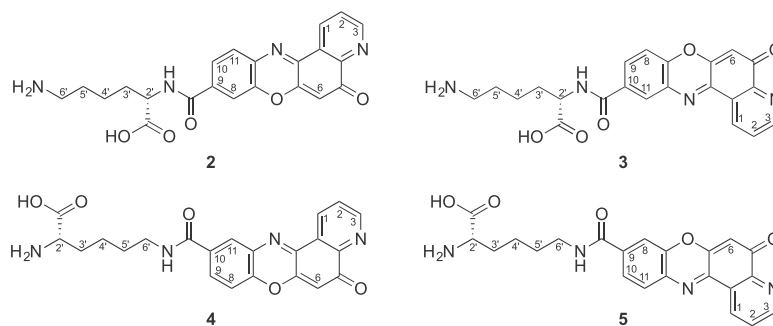
As showed in Table 3, the L-lysine side chains significantly interact with some DNA bases and their α - and ϵ -amino and/or carboxy groups seem to be involved in strong interactions. It is to note that one of the diastereotopic hydrogens belonging to the 3'-CH₂ group of the compounds **2** and **3** undergoes a shift larger than the other one ($\Delta H_b = 0.14$ and 0.04 ppm, respectively). Compound **5**, which shows a more significant shift of the chromophore protons, also displays a large shift of protons H_{2'}, H_{3'} and H_{6'} of the L-lysine ($\Delta H_{2'} = 0.32$, $\Delta H_{3'} = 0.22$ and $\Delta H_{6'} = 0.76$ ppm, respectively), suggesting a strong perturbation of the DNA double-helical

structure. This result also is in line with the observed larger cytotoxic effect of **5** on the tumor cell lines.

2.7. Computational studies

In order to rationalize the observed biological results and gain more insight into the intercalation modality of **2–5**, the supramolecular complexes of titled compounds with DNA were investigated by molecular docking. *Ab initio* calculations were also performed on the model “sandwich” complexes of pyridophenoxazinones-L-lysine conjugates with flanking DNA base pairs to establish how the entity of the two forces contributing to the π - π stacking (dispersion and charge-transfer interactions) affects the binding of compounds

Table 3
Proton chemical shift assignments of unbound **2–5** and their comparison with the corresponding **2–5**/[d(GAAGCTTC)]₂ complexes.



Ligand-Unbound Aromatic Protons (δ)								Ligand/[d(GAAGCTTC)] ₂ Complex Aromatic Protons (δ)				
	H ₁	H ₂	H ₃	H ₆	H ₈	H _{9/10}	H ₁₁	H ₁	H ₂	H ₃	H ₆	H _{8,9/10,11}
2	8.77	7.71	8.77	6.45	7.71	7.59	7.59	8.70	7.55	8.53	6.30	7.44–48
3	8.58	7.54	8.53	6.58	7.11	7.70	7.54	8.49	7.54	8.60	6.24	7.44–48
4	8.65	7.65	8.61	6.36	7.18	7.66	7.65	8.68	7.62	8.68	6.26	7.44–48
5	8.80	7.74	8.83	6.49	7.74	7.59	7.53	8.68	7.52	8.63	6.11	7.44–48

Ligand Unbound Aliphatic Protons (δ)						Ligand/[d(GAAGCTTC)] ₂ Complex Aliphatic Protons (δ)				
	H _{2'}	H _{3'}	H _{4'}	H _{5'}	H _{6'}	H _{2'}	H _{3'}	H _{4'}	H _{5'}	H _{6'}
2	4.27	1.86 _a 1.80 _b	1.44	1.73	2.95	4.38	1.86 _a 1.94 _b	1.54	1.28	2.92
3	4.18	1.81 _a 1.71 _b	1.38	1.62	2.91	4.23	1.81 _a 1.75 _b	1.42	1.65	2.93
4	3.61	1.78	1.36	1.55	3.22	3.65	1.82	1.52	1.65	3.26
5	3.59	1.78	1.57	1.64	3.27	3.91	1.56	1.57	1.64	4.03

a and b indicate CH₂ diastereotopic protons.

to DNA. Autodock 4.2 [53] was used to set up and perform docking experiments. This software has been reported to accurately reproduce the experimental binding conformation to nucleic acids of a series of small ligands (minor groove binders and intercalators) [54,55]. The d(GAAGCTTC)₂ octamer complexed with AMD (PDB code = 209D) [56] was selected for docking experiments. From a total of 200 independent docking runs, AutoDock gave well-clustered results, which were chosen on the basis of the lowest docking energy (ΔG_{bind}) and the highest frequency of occurrence (f_{occ}). Fig. 5 shows the most potent compounds **2–5** intercalated via the major groove of the 5'-GC-3' binding site with their carboxamide side chain lying in the major groove. The carboxamide side chain is oriented perpendicularly to the planar aromatic system and fits well into the interior of the major groove. The pyridophenoxazinone system intercalates with a standard stacking distance of about 3.4 Å to both G•C base pairs. It is to note that the chromophore of **3** and **4** lays in a flipped orientation rotated 180° respect to that of **2** and **5**, whereas the carboxamide side chain of all compounds projects in the same position of DNA. The carboxamide adopts a dihedral angle [C(pyridophenoxazinone)-C(pyridophenoxazinone)-C(C=O)-O(C=O)-)] of 121° with respect to the planar pyridophenoxazinone system. The positively charged pyridine nitrogen of all ligands forms two hydrogen bonds (H-bonds) with both the O4' atom in the deoxyribose ring of C5 residue and the O5' atom of the phosphate backbone located between G4 and C5 residues. These H-bonding interactions are in agreement with the H₁, H₂ and H₃ shifts observed in ¹H NMR spectra under the **2–5**/[d(GAAGCTTC)]₂ complex formation, being the shifts in **2** and **5** larger than **3** and **4**. Table S1 of Supplementary data illustrates the effect of H-bond strength on the H₁, H₂ and H₃ chemical shift differences in all ligand bounded and unbound DNA complexes.

As regards the carboxamide side chain, which adopts a *gauche-gauche* arrangement, the 6'- or 2'-NH₃⁺ group of **2–5** makes H-bonding interactions with the O6 atom of G4, O4 atom of T14 and both adenine A3 and cytosine C13 NH₂ group. The negatively charged environment of the major groove intercalation site therefore indirectly generates a favorable side-chain orientation for H-bond formation to G4, T14, A3 and C13. In addition, the 1'-COO⁻ group of **4** and **5** engages in a further charge-reinforced H-bond with the adenine A3 NH₂ group. Finally, the hydrogen of the electron-poor amide 2'- or 6'-NH group of all ligands is within H-bonding distance from the NH₂ of cytosine C13. Consistently with the reported intercalation models, when ligand/d(GAAGCTTC)₂ complexes take place, most of the protons of carboxamide side chains shift in the ¹H NMR spectra (Table 3). In the **2**/d(GAAGCTTC)₂ and **5**/d(GAAGCTTC)₂ complexes, the 2'-CH₂ protons show a very large shift (0.11 and 0.32 ppm, respectively) according to the formation of H-bonding interactions between the 2'-NH amide and 2'-NH₃⁺ groups and C13, G4, T14, and A3 DNA bases. Moreover, the change of chemical shift of one of the diastereotopic 3'-CH₂ protons of **2** and **3** in complex with the DNA octamer (Table 3) seems due to a frozen, stable conformation of the chain where the two protons experience a different chemical environment, being the proton H₆ facing towards cytosine C13.

To investigate how the entity of the π - π stacking interaction energy, i.e. dispersion forces and charge-transfer interactions, affects the binding of **2–5** to DNA base pairs, the ligand/DNA complexes generated by docking simulations were subjected to quantum mechanical single point energy calculations. In order to derive a simplified model for such calculations, compounds **2–5** and their flanking base pairs were extracted from the ligand/DNA complexes. The deoxyribose rings of the flanking base pairs were

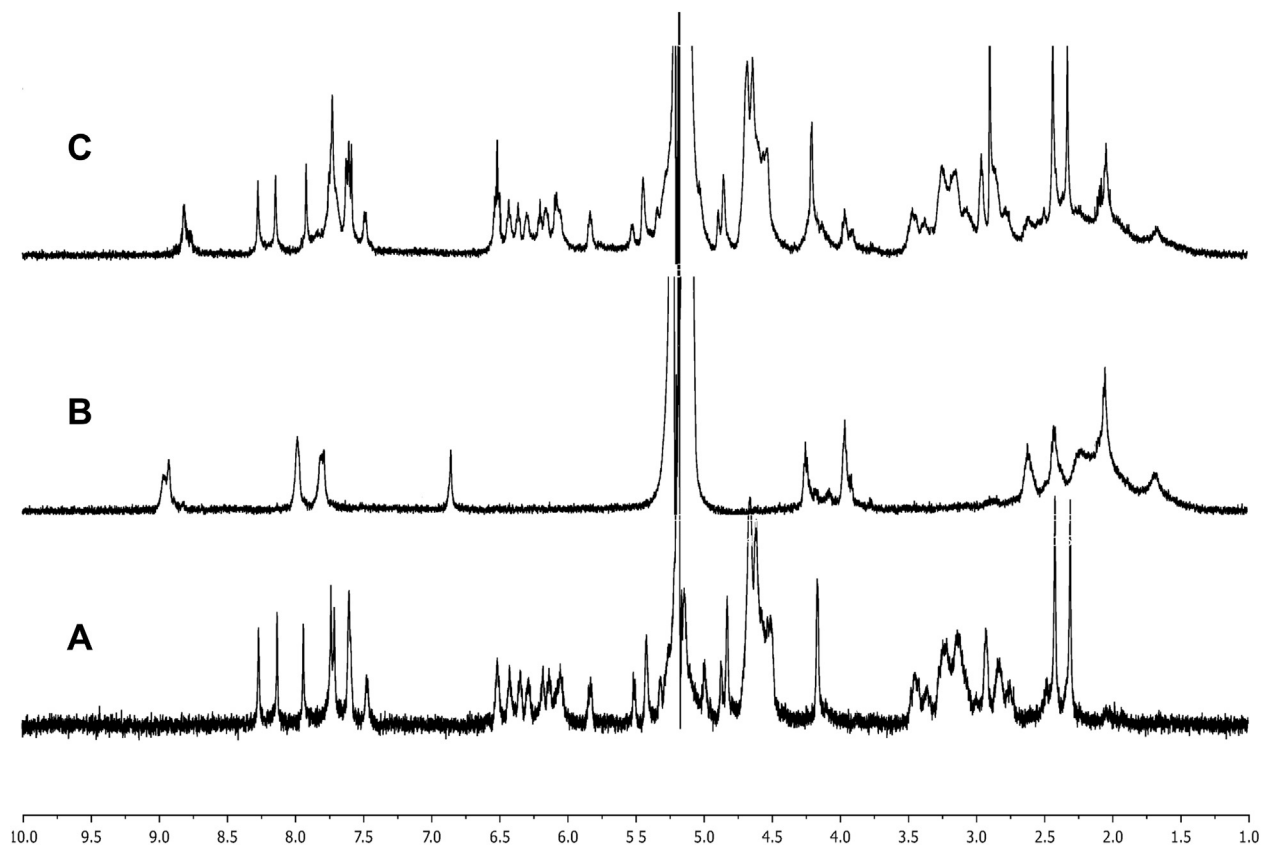


Fig. 4. ^1H NMR spectrum in phosphate buffer/ D_2O pH 7 of the (A) octamer $\text{d}(\text{GAAGCTTC})_2$, (B) **5**, and (C) **5**/[$\text{d}(\text{GAAGCTTC})_2$] $_2$ complex.

replaced by methyl groups, and the carboxamide side chains at 9 and 10 positions of pyridophenoxazinones were substituted by methylamide groups because the chains are considered to be non-participating groups in π - π stacking interactions. The energies of molecules **2**-**5**, C-G base pair, and G-C base pair were optimized separately at the HF/6-31G** level of theory in Jaguar 9.0 software package [57]. The original complexes were then replaced with the geometry of optimized parts (Fig. 6, model **A**, representative of compounds **2** and **5**, and model **B**, representative of compounds **3** and **4**). Models **A** and **B** were then subjected to a single-point energy calculation at the LMP2 (local Møller-Plesset second-order perturbation theory) level of theory by using the 6-31G* basis set. The LMP2 method [58] is known to minimize basis set superposition error (BSSE), and therefore counterpoise correction [59] was not included in the calculations.

The in vacuo π - π stacking interaction energy was then calculated as $E_{\text{int,vac}} = E_{\text{complex,vac}} - E_{\text{ligand,vac}} - E_{\text{bp,vac}}$, where $E_{\text{complex,vac}}$, $E_{\text{ligand,vac}}$, and $E_{\text{bp,vac}}$ are the corresponding LMP2/6-31G* calculated energies of complex, ligand, and DNA base pairs at their normal distance in the absence of intercalator (Table 4). Similarly, the energy of the π - π staking interaction was also calculated in water ($E_{\text{int,aq}}$) using the polarized continuum model.

As π - π stacking mainly originates from dispersion and charge transfer interactions, we calculated the dispersion and charge transfer contributions to make a direct quantitative comparison of their roles in the binding of pyridophenoxazinones to DNA complex. The dispersion (electron correlation) interaction (E_{corr}) was defined as the difference of energy calculated by LMP2 and HF methods at the 6-31G* level, $E_{\text{corr}} = E_{\text{int(LMP2)}} - E_{\text{int(HF)}}$ (Table 4). The energy associated with charge transfer was obtained as result of natural bond orbital (NBO) analysis in Jaguar [57]. The NBO analysis

was performed at the HF/6-31G** level of theory and presented as E_{CT} in Table 4.

As shown in Table 4, models **A** and **B** share comparable dispersion energies, indicating that this kind of interaction is isotropic (i.e. independent of spatial orientation) and proportional to the geometrical overlap of the stacked systems. Analysis of the E_{CT} column, on the other hand, suggests that the charge transfer stabilization energy is greater by 4.10 kcal/mol for pyridophenoxazinones represented by model **A** in comparison to pyridophenoxazinones in model **B**. These results indicate that the charge transfer interactions play a much more important role in the stabilization of the complexes between **2/5** and DNA than between **3/4** and DNA, which might help to explain the superior cytotoxicity of compounds **2** and **5** versus the corresponding **3** and **4**.

2.8. Inhibition of the catalytic activity of Topo II α in vitro

The relaxation of supercoiled plasmid DNA by human Topo II α was studied in the presence of different concentrations of **2** or **5**. Compound **5** diminished the relaxation reaction by 50% at a concentration of 0.7 μM and totally inhibited the Topo II-mediated relaxation at 1.5 μM (Fig. 7, right). The closely related compound **2** also inhibited the catalytic activity of Topo II α , but to a lesser extent. Approximately 1 μM **2** was required to inhibit the relaxation reaction by 50%, whereas 2 μM was needed to completely inhibit the catalytic activity (Fig. 7, left).

2.9. Induction of Topo II α and Topo II β cleavable complexes in vitro

The biologically active **2** and **5** are able to induce cleavable complexes between Topo II α and pBR322 plasmid DNA (Fig. 8) more

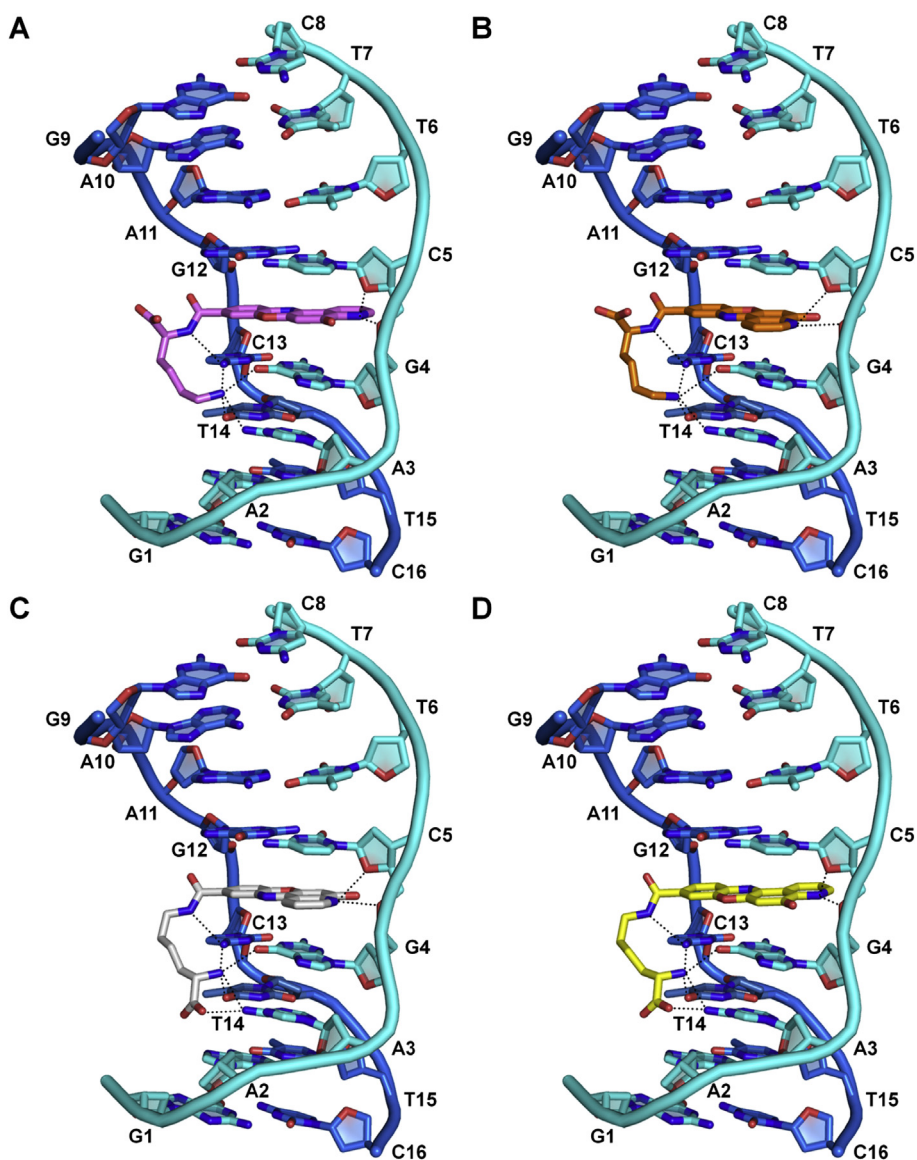


Fig. 5. Pyridophenoxazinones-1-lysine conjugates **2** (A, magenta), **3** (B, orange), **4** (C, white), and **5** (D, yellow) intercalated into 5'-GC-3' base pairs of the DNA octamer d(GAAGCTTC)₂. Black dashed lines indicate H-bonds. (For interpretation of the references to color in this figure legend, the reader is referred to the Web version of this article.)

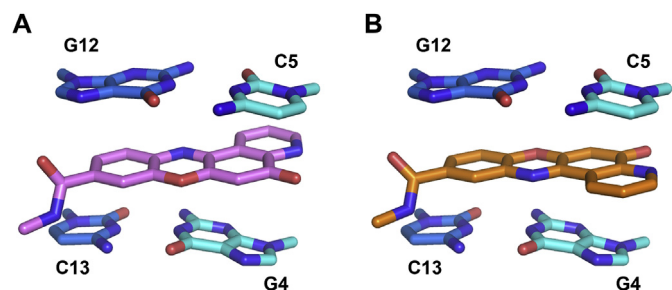


Fig. 6. Intercalation complex model containing simplified structures of **2/5** (model A) and **3/4** (model B) and their flanking base pairs for *ab initio* calculations.

effectively than amsacrine (AMSA). The formation of cleavable complex with Topo II α was dose-dependent, reaching a maximum in the presence of 1–5 μ M **2** and **5**. At higher concentrations, the binding of two carboxamides to DNA generated a characteristic

biphasic pattern, which is typical of compounds that are strong DNA binders [60,61]. Therefore, both **2** and **5** can be considered to be Topo II α poisons.

It is notable that Topo II poisons are used widely in the clinic to treat a variety of cancers; however, their utility is hampered by severe adverse side effects including cardiac myopathies and secondary malignancies [9], which appear to be correlated with their ability to poison Topo II β [12,13]. Hence, finding drugs specifically targeting Topo II α with low Topo II β -mediated toxicity/carcinogenicity is being actively pursued [62]. Thus, DNA cleavage assay experiments were also carried out to determine whether compound **5** stabilized the cleavable complex induced by Topo II β . Results showed that **5** was more selective in inducing linear DNA formation by acting on Topo II α than on Topo II β (Fig. S16 in Supplementary data). In order to rationalize the observed inhibitory effect on the enzymatic activity of Topo II α , **5** was docked into the recently solved X-ray crystal structure of the human Topo II α /DNA/etoposide ternary complex (PDB code = 5GWK) [63]. The overall results showed that **5** is able to stabilize Topo II α /DNA cleavage

Table 4
 π - π Stacking interaction energies of models **A** and **B**.

Model	$E_{\text{int, vac}}^a$ (kcal/mol)	$E_{\text{int, aq}}^a$ (kcal/mol)	E_{corr}^b (kcal/mol)	E_{CT}^c (kcal/mol)
A	-6.24	-12.15	-28.46	-16.28
B	-6.11	-10.89	-27.85	-12.18

^a E_{int} is derived from LMP2/6-31G* single point energy calculations.

^b $E_{\text{corr}} = E_{\text{int(LMP2/6-31G}^*)} - E_{\text{int(HF/6-31G}^*)}$.

^c The magnitude of the charge transfer as estimated by NBO analysis at HF/6-31G** level.

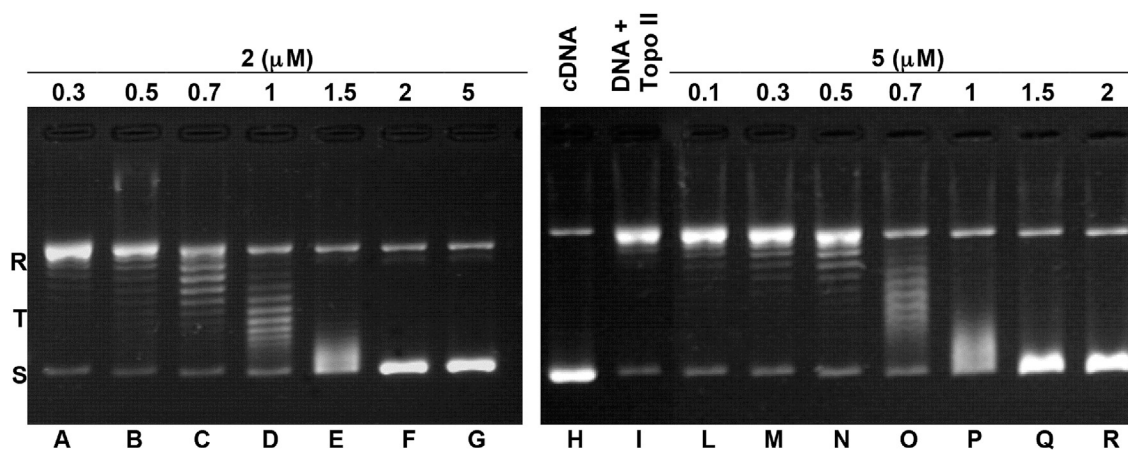


Fig. 7. Inhibition of the catalytic activity of purified DNA Topo II α by L-lysine conjugates **2** and **5** as measured by relaxation. Supercoiled pBR322 plasmid DNA (lane H) was relaxed by purified Topo II α in the absence (lane I) or presence of **2** at 0.3, 0.5, 0.7, 1, 1.5, 2 and 5 μ M (lanes A-G) or with **5** at 0.1, 0.3, 0.5, 0.7, 1, 1.5, and 2 μ M (lanes L-R). The resulting topological forms of DNA were separated by gel electrophoresis. S, supercoiled DNA; R, relaxed DNA; T, DNA topoisomers. Data shown are typical of three independent experiments.

complex (See more details and Fig. S17 in Supplementary data). Modeling studies also suggested that the enhanced Topo II α specificity of **5** may result from interactions with a serine residue that is present in Topo II α , but not in Topo II β (Fig. S18 in Supplementary data). Thus, compound **5** was chosen to further investigate its anticancer mechanism.

2.10. DNA damage induced by compound 5

Considering that compound **5** behaves as an intercalative Topo II inhibitor, we further investigated the action mode of **5** with MCF-7 cells by observing comet tails in the single cell gel electrophoresis (comet assay). The assay gives an image of the alterations that have happened in the chromatin organization in a single cell. It is considered a more correct fashion of detection of nuclear modifications in a cell population [64,65]. Compound **5** provoked lesions in DNA and significantly increased the comet tail lengths with increasing concentration. Fig. 9A shows an increase in comet formation following treatment with compound **5** at concentrations ranging from 1 to 10 μ M, while no comet formation was observed in untreated cells. Fig. 9B shows the comet lengths in pixels with respect to the concentration of **5**. In cells treated with 10 μ M **5**, the tail length was ~50% when compared with the tail length of untreated MCF-7 cells, which is nearly 8% ($p < 0.05$). From these data, it can be concluded that **5** could induce severe DNA damage in breast cancer cells.

To gain more insight into the induction of DNA damage of compound **5**, we monitored the levels of phosphorylated histone H2AX (γ H2AX) in MCF-7 cells treated with **5**. γ H2AX is known as a biomarker for double strand breaks in DNA [66–68]. As shown in Fig. 9C, the levels of γ H2AX in the **5**-treated MCF-7 cells were clearly augmented, indicating that compound **5** was a potent DNA-damaging agent.

2.11. Compound 5 induces G2/M phase cell cycle arrest and apoptosis in MCF-7 cells

The effect of **5** on the cell cycle progression of MCF-7 cells was evaluated after continuous exposure to 0.01 and 0.1 μ M drug concentrations for 12 h, 24 h and 48 h, respectively. Cultures treated with **5** at 0.01 μ M exhibited only a minimal deviation from control cell cycle distribution (data not shown). Exposure to **5** at 0.1 μ M provoked a visible perturbation of cell cycle progression (Fig. 9D). A noticeable increase in the percentage of cells in G2 phase, and an important diminution in cell number over control was detected after 24 and 48 h (control: 17.00% \pm 3.01%; 24 h: 26.00% \pm 7.5%; 48 h: 48.77% \pm 9.55%), outlining a G2 phase accumulation. Meanwhile, G0/G1 dropped considerably from 51.70% \pm 6.99%–42.50% \pm 9.41% and the population in S phase was reduced to 8.73% \pm 0.3% during 48 h incubation. These results suggest that G2/M phase arrest accounts for the antiproliferative effect of **5** observed in MCF-7 cells.

3. Conclusions

Novel pyridophenoxazinone-L-lysine conjugates (compounds **2–5** and **2'-5'**) were designed, synthesized and evaluated for their anticancer activity against a wide variety of hematological and solid human tumor cell lines. All the compounds exhibited high antiproliferative activity, displaying potency equal or larger of Doxo and VP-16. **2** and **5** were the most potent compounds of the series with IC₅₀ values ranging between 0.001 and 0.008 μ M against the majority of solid cell lines and 0.01 and 0.15 μ M against human leukemia cell lines. The interaction with DNA, studied by optical spectrophotometry and ¹HNMR spectroscopy, showed that these compounds are strong DNA intercalators. Docking studies suggested that **2–5** intercalate at the 5'-GC-3' binding site with their

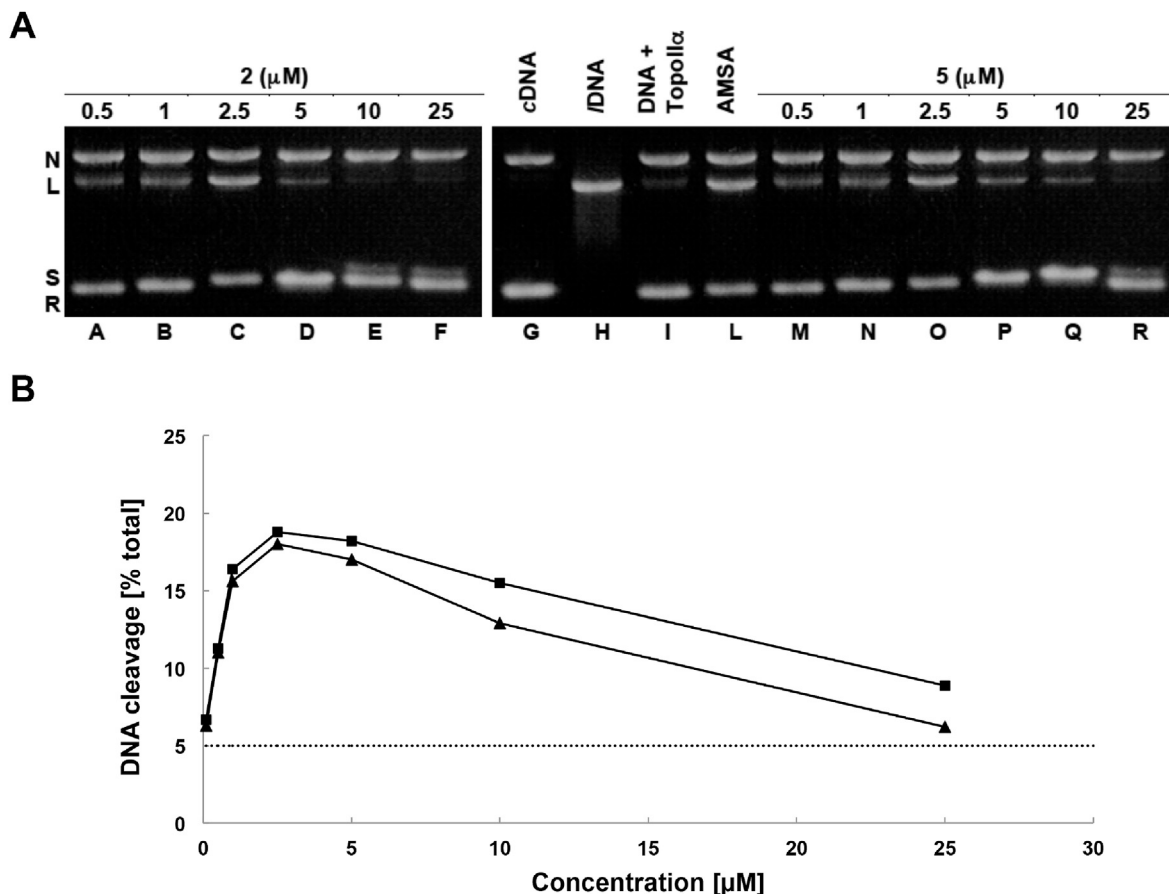


Fig. 8. The influence of **2** and **5** on the formation of covalent DNA/Topo II α complexes. (A) Supercoiled pBR322 plasmid DNA (lane G) was incubated with purified Topo II α in the absence (lane I) or in the presence of 10 μ M AMSA (lane L) or with 0.5, 1, 1.5, 2, 5, and 10 μ M **2** (lanes A–F) or **5** (lanes M–R). The resulting DNA/Topo II α complexes were digested by proteinase K, and the different topological forms of DNA were separated by agarose gel electrophoresis in the presence of EtBr. Lane H, linearized pBR322 DNA. S, supercoiled DNA; R, relaxed DNA; L, linear DNA; N, nicked circular DNA. Data shown are typical of three independent experiments. (B) Topo II α -mediated DNA cleavage in the presence of L-lysine conjugates **2** and **5**. Plasmid DNA and purified Topo II α were incubated with different concentrations of **2** or **5**, and the formation of linear DNA determined by gel densitometry. Data shown are the averages of three independent experiments. ▲, cleavage induced by **2**; ■, cleavage induced by **5**. The dotted line indicates the background levels of cleavable complexes formed in the absence of drug.

carboxamide side chain lying in the major groove. *Ab initio* calculations of the relative contributions of dispersion and charge transfer demonstrated that the charge transfer interactions play a much important role in the stabilization of the complex between compounds **2** and **5** and flanking base pairs, which might help to explain their high cytotoxicity. DNA unwinding, relaxation and cleavage assays, performed on **2** and **5**, validated their intercalating properties and showed a selective inhibitory effect on the catalytic activity of human Topo II α over Topo II β . Moreover, **2** and **5** stabilized cleavable complexes between Topo II α and DNA, indicating that they can be considered as Topo II α poisons. Further study indicated that compound **5** significantly induced DNA damage and arrested cancer cells at G2/M phase. All together, these characteristics indicate that this new series of L-lysine-conjugated pyridophenoxazinones, acting in multimodal way, are endowed with advantageous antitumor therapeutic potential. The molecule **5** provides interesting opportunities to develop novel DNA-targeted anticancer agents.

4. Experimental protocols

4.1. Chemistry

Reagents, starting materials, and solvents were purchased from

commercial suppliers and were used as received. The purity of compounds was checked by ascending TLC on Merck's silica gel plates 60 F₂₅₄ (0.25 mm) using UV and fluorescent light or ninhydrin (sol. 0.25% in MeOH). Melting points were determined by a Kofler apparatus and are uncorrected. The purity of the synthesized compounds was established by combustion analysis with a Thermo Scientific (Flash 2000) analyzer and was within $\pm 0.4\%$. Mass measurements were performed in positive ion mode using a Micromass electrospray ionization instrument (LC-T; Waters, UK). UV spectra were recorded on Varian Cary 5000 UV–Vis–NIR Spectrophotometer. HPLC analysis was performed by a RP-HPLC on a semi-preparative C18-bonded silica column (Phenomenex, Jupiter, 250 \times 10 mm) using a Shimadzu SPD 10 A UV/VIS detector. MW CEM Discover apparatus, 2.45 GHz, CEM Corporation, NC, USA was used to perform the MW assisted synthesis. NMR measurements (data reported in ppm) were performed on a Bruker AMX-500 spectrometer equipped with a Bruker X-32 computer, using the UxNMR software package. NMR spectra were measured at 500 MHz (^1H) and 125 MHz (^{13}C). The chemical shifts are referenced to $^{13}\text{CDCl}_3$ and CDCl_3 solvent signals at 77.0 and 7.26 ppm, respectively. Standard pulse sequences were employed for magnitude COSY, HMQC and HMBC experiments were optimized for $^1\text{J}_{\text{C-H}}$ 135 Hz and $^2,3\text{J}_{\text{C-H}}$ 10 Hz, respectively. Me_4Si was used as the internal reference.

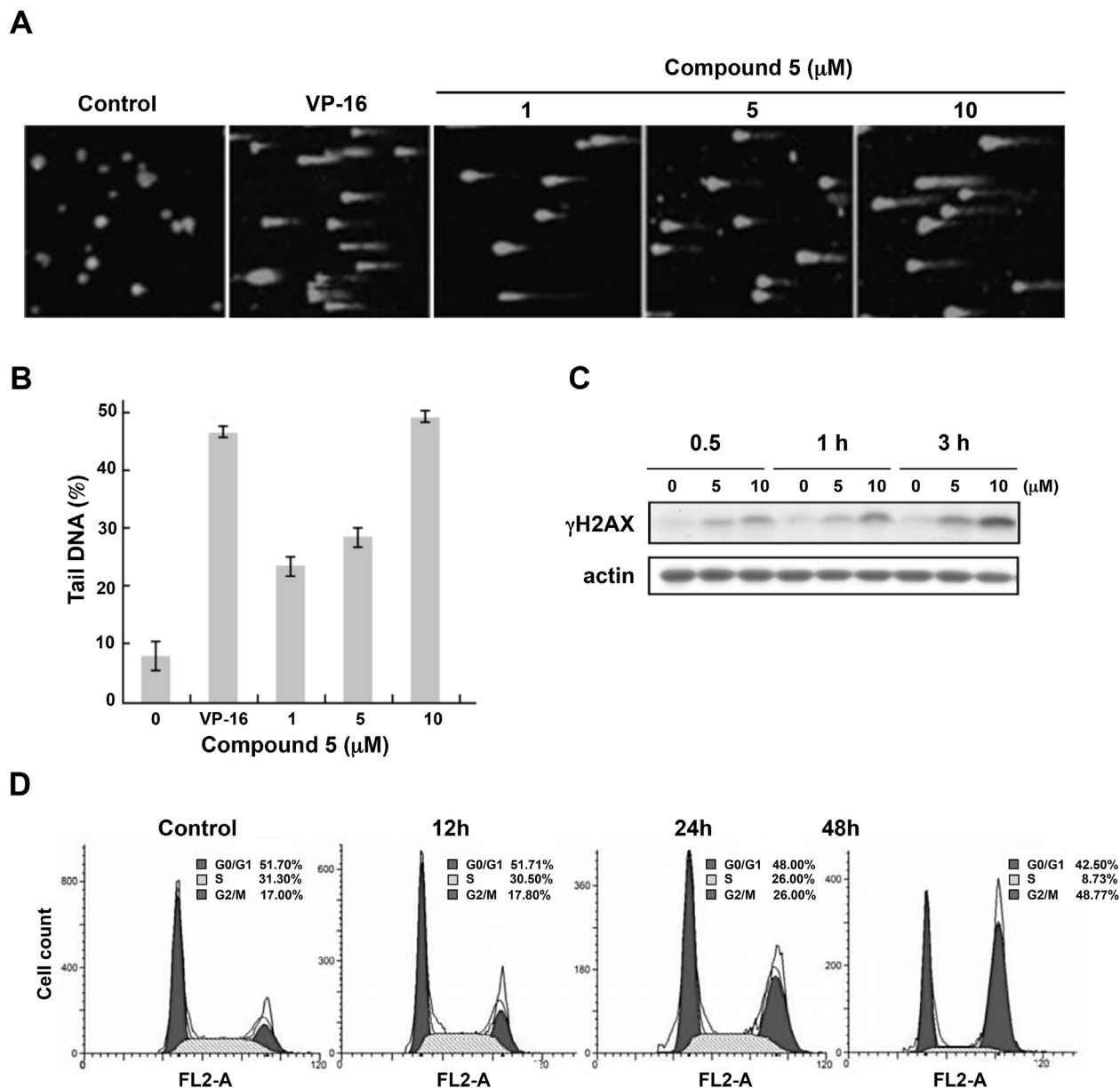


Fig. 9. Compound **5** induces DNA double strand break in MCF-7 cells. Cells were seeded in 24-well tissue-culture plates and after 70% confluence were treated with **5** for 24 h. After treatment, cells were processed for comet assay as detailed under Experimental protocols section. (A) Images of MCF-7 cells after treatment with the negative control (nontreated), VP-16 (positive control, 10 μM), and compound **5** (1, 5, and 10 μM) showing comet formation. (B) Graphical representation of the selected comet lengths of MCF-7 (control and treated cells) in pixels with corresponding to concentration. (C) MCF-7 cells were incubated with DMSO or 5 or 10 μM **5** for the indicated time periods. After treatment, cells were harvested and lysed for detection of the expression of γH2AX via western blotting. (D) **5**-induced cell cycle arrest at the G2/M phase in MCF-7 cells. Cells were treated with vehicle and 0.1 μM **5** for 12, 24, and 48 h, and cell cycle distribution was assessed by flow cytometry.

4.1.1. Synthesis of 5-oxo-5H-pyridophenoxazine carboxylic acid (1, 1', 1'', 1''')

4.1.1.1. Conventional procedure. The solutions of 3-amino-4-hydroxybenzoic acid and 3-hydroxy-4-amino-benzoic acid (0.01 mol) in methanol-acetic acid (50:50; vv, 10 mL) were added, respectively, dropwise to an equimolar solution of quinolin-5,8-dione (0.01 mol) in acetic acid (10 mL). The mixtures were stirred and refluxed for 12 h and evaporated in vacuo. The solid residues, extracted in CHCl₃, were purified on silica gel column (CHCl₃:CH₃OH, 8:2 as eluent). The pyridophenoxazinones **1-1'** and **1''-1'''** were obtained with yields 10–12% and 20–25%, respectively. To increase the very poor yields of compounds **1** and **1''**, the reported reactions were repeated in presence of Co(II) acetate

(0.01 mol) and gently warmed until the dark color showed the complex formation. After 12 h at refluxing temperature, the reaction mixtures were evaporated in vacuo and the solid residues, dissolved in CHCl₃, were washed with acidified water (HCl 6 N) to break the Co(II)-complex and extracted in CHCl₃. After purification on silica gel column (CHCl₃:CH₃OH, 8:2 as eluent), the pyridophenoxazinones **1-1'** and **1''-1'''** were obtained with yields 16–18% and 20–23%, respectively.

4.1.1.2. MW assisted procedure. In MW tubes, the solutions of quinolin-5,8-dione (0.1 mmol), cobalt acetate and 3-amino-4-hydroxybenzoic acid or 3-hydroxy-4-amino-benzoic acid (0.1 mmol) in acetic acid (5 mL) were added, respectively. The tubes

were shook to dissolve the reagents until to obtain dark orange solutions and were irradiated for 15 min at 50 W of power. The reaction was stopped and oxygen was bubbled in the tube for 1 min. After 15 min, the mixture was evaporated under reduced pressure, washed with THF and filtered on Whatmann paper. Chromatography of the products on silica gel columns (CHCl₃/MeOH, 8:2 as eluent) afforded the pure compounds. The yields of **1** and **1''** were 35% and 40%, respectively. According to the above reported procedure compounds **1'** and **1'''** were prepared. In this case, no cobalt acetate was added to reaction mixture allowing the amine groups of the 3-Amino-4-hydroxybenzoic acid and 3-hydroxy-4-aminobenzoic acid aminophenols to attack the quinoline quinone 8-carbonyl group. Under the reported conditions the following products were obtained whit yields 50%, 67%.

4.1.2. 5-Oxo-5H-pyrido[3,2-a]phenoxazine-9-carboxylic acid (**1**)

Yield 38%; ¹H NMR (500 MHz, CDCl₃) δ 9.11 (dd, *J* = 4.5, 1.5 Hz, 1H), 9.05 (dd, *J* = 8.1, 1.5 Hz, 1H), 7.90 (d, *J* = 7.9 Hz, 1H), 7.86 (m, 2H), 7.74 (dd, *J* = 8.1, 4.5 Hz, 1H) 6.65 (s, 1H); ¹³C NMR (100 MHz, CD₃OD) δ 180.53, 163.95, 154.34, 149.93, 148.27, 139.92, 136.55, 129.81, 126.12, 123.56, 122.17, 120.13, 118.33, 111.45, 105.39; MS (ESI), *m/z*: 293 (M⁺+1); Anal. Calcd. for C₁₆H₈N₂O₄: C, 65.76%; H, 2.76%; N, 9.59%; Found: C, 65.65%; H, 2.77%; N, 9.63%.

4.1.3. 5-Oxo-5H-pyrido[2,3-a]phenoxazine-9-carboxylic acid (**1'**)

Yield 40%; ¹H NMR (600 MHz, CDCl₃) δ 9.08 (dd, *J* = 4.5, 1.7 Hz, 1H), 8.64 (dd, *J* = 8.1, 1.7 Hz, 1H), 8.12–7.96 (m, 2H), 7.92 (s, 1H), 7.90–7.88 (dd, *J* = 8.1, 4.5 Hz, 1H), 6.53 (s, 1H); ¹³C NMR (100 MHz, CD₃OD) δ 182.12, 165.44, 161.03, 154.72, 153.09, 151.05, 147.88, 143.86, 138.35, 134.31, 131.35, 128.37, 123.75, 122.05, 118.12, 107.71; MS (ESI), *m/z*: 293 (M⁺+1); Anal. Calcd. for C₁₆H₈N₂O₄: C, 65.76%; H, 2.76%; N, 9.59%; Found: C, 65.78%; H, 2.73%; N, 9.64%.

4.1.4. 5-Oxo-5H-pyrido[3,2-a]phenoxazine-10-carboxylic acid (**1''**)

Yield 50%; ¹H NMR (600 MHz, CDCl₃) δ 9.10 (m, 1H), 9.03 (m, 1H), 8.36 (m, 1H), 8.14 (m, 1H), 7.98–7.88 (m, 2H), 7.62 (s, 1H), 6.63 (s, 1H); ¹³C NMR (150 MHz, DMSO-*d*₆) δ 182.33, 165.19, 161.23, 153.66, 151.93, 147.05, 144.04, 138.77, 133.47, 133.14, 130.75, 126.36, 123.99, 123.67, 115.71, 105.53; MS (ESI), *m/z*: 293 (M⁺+1); Anal. Calcd. for C₁₆H₈N₂O₄: C, 65.76%; H, 2.76%; N, 9.59%; Found: C, 65.83%; H, 2.71%; N, 9.49%.

4.1.5. 5-Oxo-5H-pyrido[2,3-a]phenoxazine-10-carboxylic acid (**1'''**)

Yield 67%; ¹H NMR (400 MHz, CDCl₃) δ 9.16 (dd, *J* = 4.6, 1.7 Hz, 1H), 8.56 (dd, *J* = 7.9, 1.7 Hz, 1H), 8.40 (d, *J* = 1.7 Hz, 1H), 8.17 (dd, *J* = 8.5, 1.7 Hz, 1H), 7.91 (dd, *J* = 7.9, 4.6 Hz, 1H), 7.62 (d, *J* = 8.5 Hz, 1H), 6.57 (s, 1H); ¹³C NMR (150 MHz, DMSO-*d*₆) δ 182.74, 165.01, 164.34, 154.57, 150.82, 150.68, 139.54, 138.87, 136.73, 135.91, 129.99, 129.63, 127.72, 126.91, 118.72, 106.90; MS (ESI), *m/z*: 293 (M⁺+1); Anal. Calcd. for C₁₆H₈N₂O₄: C, 65.76%; H, 2.76%; N, 9.59%; Found: C, 65.86%; H, 2.81%; N, 9.54%.

4.1.6. (S)-tert-Butyl 2-amino-6-((tert-butoxycarbonyl)amino)hexanoate (**C**)

A solution of commercial Fmoc-L-lys(Boc)OH (**A**) (1.5 g, 3.2 mmol) in CH₂Cl₂ (6.5 mL) was added with a solution of tert-butyl trichloroacetimidate (1.15 mL, 6.4 mmol) in cyclohexane (6.5 mL) and with boron trifluoride diethyl etherate (64 μL, 3.2 mmol). The mixture was stirred for 24 h at room temperature and, subsequently, the solvent was evaporated under reduced pressure and replaced by CHCl₃. This solution, washed with Brine, dried (Na₂SO₄) and evaporated under reduced pressure gave a crude residue that, purified by chromatography on a silica gel column (CHCl₃ as eluent), afforded the oily product (S)-tert-butyl 2-(((9H-fluoren-9-yl)methoxy)carbonyl)amino)-6-((tert-

butoxycarbonyl)amino)hexanoate (**B**) (1.64 g, 3.14 mmol) used without further purification. Yield 90%; ¹H NMR (500 MHz, CDCl₃) δ 8.83 (s, 1H), 8.43 (s, 1H), 7.78–7.77 (m, *J* = 7.5 Hz, 2H), 7.62–7.61 (d, *J* = 7.3 Hz, 2H), 7.41 (t, *J* = 7.4 Hz, 2H), 7.32 (t, *J* = 7.4 Hz, 2H), 5.38 (d, *J* = 7.1 Hz, 1H), 4.56 (bs, 1H), 4.35–4.32 (m, 2H), 4.24 (m, 2H), 3.11 (bs, 1H), 1.83 (dd, *J* = 14.6, 9.5 Hz, 1H), 1.67 (m, 1H), 1.59–1.19 (m, 22H); ¹³C NMR (50 MHz, CDCl₃) 172.13, 164.24, 156.32, 144.04, 141.51, 127.84, 127.21, 125.25, 120.06, 82.09, 79.10, 66.76, 53.96, 46.87, 39.84, 31.95, 29.19, 28.00, 27.59, 21.84; MS (ESI), *m/z*: 525 (M⁺+1); Anal. Calcd. for C₃₀H₄₀N₂O₆: C, 68.68%; H, 7.68%; N, 5.34%; Found: C, 68.70%; H, 7.70%; N, 5.36%.

A solution of compound **B** (1.64 g, 3.13 mmol) in CH₃CN (51 mL) at 0 °C was added with piperidine (1.12 mL, 3.13 mmol). The mixture was stirred for 30 min and warmed up to room temperature. After 3 h, the solvent was evaporated under reduced pressure and replaced by CHCl₃. The solution washed with Brine, dried (Na₂SO₄), evaporated under reduced pressure gave a crude residue that, purified by chromatography on silica gel column (CHCl₃:MeOH, 9:1 as eluent) afforded the oily product **C** (926 mg, 3.07 mmol). Yield 98%; ¹H NMR (500 MHz, CDCl₃) δ 4.65 (s, 1H), 3.26 (dd, *J* = 7.3, 5.5 Hz, 2H), 3.08 (d, *J* = 6.2 Hz, 2H), 1.66 (m, 2H), 1.65 (m, 2H), 1.64 (m, 18H); ¹³C NMR (125 MHz, CDCl₃) δ 176.20, 156.73, 81.27, 79.34, 55.09, 40.50, 34.67, 29.90, 28.49, 28.13, 22.90; MS (ESI), *m/z*: 303 (M⁺+1); Anal. Calcd. for C₁₅H₃₀N₂O₄: C, 59.57%; H, 10.00%; N, 9.26%; Found: C, 59.60%; H, 10.01%; N, 9.23%.

4.1.7. (S)-tert-Butyl 6-amino-2-((tert-butoxycarbonyl)amino)hexanoate (**F**)

A solution of commercial Boc-L-lys(Cbz)OH (**D**) (1 g, 2.63 mmol) in CH₂Cl₂ (5.26 mL) and tert-butyl trichloroacetimidate (0.94 mL, 5.26 mmol) in cyclohexane (5.26 mL) was added with boron trifluoride diethyl etherate (52.6 μL, 2.63 mmol). The mixture was stirred for 24 h at room temperature. The solvent was evaporated under reduced pressure and replaced by CHCl₃. The solution, washed with Brine, dried (Na₂SO₄) and evaporated under reduced pressure, gave a crude residue that, purified chromatographically on silica gel column (CH₂Cl₂ as eluent) afforded the oily product (S)-tert-butyl 6-(((benzyloxy)carbonyl)amino)-2-((tert-butoxycarbonyl)amino)hexanoate (**E**) (882 mg, 2.03 mmol) used without further purification. Yield 77%; ¹H NMR (500 MHz, CDCl₃) δ 7.36–7.33 (m, 5H), 5.09 (s, 2H), 5.06 (bs, 1H), 4.82 (bs, 1H), 4.15 (dd, *J* = 11.6, 6.4 Hz, 1H), 3.21–3.17 (dd, *J* = 12.7, 6.4 Hz, 2H), 1.77 (m, 1H), 1.53–1.39 (m, 23H); ¹³C NMR (100 MHz, CDCl₃) δ 171.68, 163.63, 156.22, 155.19, 136.07, 128.01, 127.57, 81.48, 79.31, 66.11, 53.34, 40.14, 31.87, 28.82, 27.81, 27.47, 21.87; MS (ESI), *m/z*: 437 (M⁺+1); Anal. Calcd. for C₂₃H₃₆N₂O₆: C, 63.28%; H, 8.31%; N, 6.42%; found: C, 63.30%; H, 8.29%; N, 6.39%.

A solution of **E** (882 mg, 2.03 mmol) in MeOH dry (8 mL) was degassed and added with 10 wt % Pd/C (43 mg, 0.406 mmol). H₂ was bubbled, and stirring was performed overnight. The reaction mixture was filtered through a Celite bed and washed with methanol. The evaporation of the solvent under reduced pressure gave the oily product **F** (552 mg, 1.83 mmol, 90% yield). Yield 90%; ¹H NMR (500 MHz, CDCl₃) δ 5.11 (m, 1H), 4.16 (m, 1H), 3.15 (m, 2H), 2.78 (m, 2H), 1.78 (m, 1H), 1.58 (m, 3H), 1.38 (m, 18H); ¹³C NMR (125 MHz, CDCl₃) δ 172.33, 155.74, 81.73, 79.52, 53.57, 40.88, 32.31, 31.06, 27.96, 27.63, 22.05; MS (ESI), *m/z*: 303 (M⁺+1); Anal. Calcd. for C₁₅H₃₀N₂O₄: C, 59.57%; H, 10.00%; N, 9.26%; found: C, 59.60%; H, 9.98%; N, 9.25%.

4.1.8. General procedure for the preparation of compounds **2–5** and **2'-5'**

Step 1. The solutions of the carboxylic acids **1-1'''** (0.50 mmol) in anhydrous THF (24 mL), at 0 °C, were added with HOBT

(1.0 mmol) in a portion, respectively. After 30 min, a solution of *L*-lys(Boc)OtBu (**C**) (0.70 mmol) in anhydrous THF (24 mL) and EDC (100 μ L, 0.56 mmol) was added to the reaction mixtures. The mixtures were stirred for 12 h at 0 °C and allowed to warm slowly to room temperature. The solvent was evaporated under reduced pressure, replaced with AcOEt and the mixtures were washed with saturated aqueous solutions of NH₄Cl, Brine and dried (Na₂SO₄). The evaporation of the solvent under reduced pressure gave the crude residues that, purified chromatographically on silica gel (CHCl₃:MeOH, 95:5 as eluent), afforded the coupling products **2a-2'a** and **3a-3'a**. The above reported procedure performed by using the acids **1-1''** and Boc-*L*-lysOtBu (**F**) yielded the corresponding compounds **4a-4'a** and **5a-5'a**.

4.1.8.1. (*S*)-*tert*-butyl 6-((*tert*-butoxycarbonyl)amino)-2-(5-oxo-5H-pyrido[3,2-*a*]phenoxazine-9-carboxamido)hexanoate (**2a**). Yield 90%; ¹H NMR (500 MHz, CDCl₃) δ 9.14 (dd, *J* = 4.7, 1.6 Hz, 1H), 9.08 (dd, *J* = 8.0, 1.6 Hz, 1H), 7.93 (d, *J* = 8.1 Hz, 1H), 7.85 (m, 1H), 7.84 (dd, *J* = 8.1 Hz, 1H), 7.76 (dd, *J* = 8.0, 4.7 Hz, 1H), 6.95 (d, *J* = 6.0 Hz, 1H), 6.68 (s, 1H), 4.69 (dd, *J* = 12.1, 6.0 Hz, 1H), 4.60 (bs, 1H), 3.15 (m, 2H), 1.99 (m, 1H), 1.83 (m, 1H), 1.57 (m, 2H). ¹³C NMR (100 MHz, CDCl₃) δ 187.39, 182.54, 172.04, 156.98, 154.17, 151.25, 148.30, 144.24, 137.69, 133.61, 131.10, 130.37, 126.46, 124.28, 115.53, 109.33, 82.62, 79.06, 53.04, 41.86, 39.69, 31.73, 29.96, 29.33, 27.98, 27.63; MS (ESI), *m/z*: 577 (M⁺+1); Anal. Calcd. for C₃₁H₃₆N₄O₇: C, 64.57%; H, 6.29%; N, 9.72%; Found: C, 64.55%; H, 6.30%; N, 9.74%.

4.1.8.2. (*S*)-*tert*-butyl 6-((*tert*-butoxycarbonyl)amino)-2-(5-oxo-5H-pyrido[2,3-*a*]phenoxazine-9-carboxamido)hexanoate (**2'a**). Yield 90%; oil; ¹H NMR (500 MHz, CDCl₃) δ 9.19 (m, 1H), 8.65 (d, *J* = 7.9 Hz, 1H), 8.18 (d, *J* = 8.1 Hz, 1H), 7.86 (s, 1H), 7.83 (dd, *J* = 8.1 Hz, 1H), 7.75 (m, 1H), 6.96 (m, 1H), 6.55 (s, 1H), 4.67 (m, 1H), 4.60 (bs, 1H), 3.13 (m, 2H), 1.98 (m, 1H), 1.84 (m, 1H), 1.57 (m, 2H), 1.51 (m, 2H). ¹³C NMR (100 MHz, CDCl₃) δ 182.22, 171.51, 170.13, 164.73, 164.27, 155.95, 153.71, 152.12, 147.76, 144.12, 134.75, 134.23, 131.37, 128.90, 128.72, 126.41, 123.85, 115.23, 107.40, 82.56, 80.55, 52.82, 39.86, 32.00, 29.59, 28.25, 27.91; MS (ESI), *m/z*: 577 (M⁺+1); Anal. Calcd. for C₃₁H₃₆N₄O₇: C, 64.57%; H, 6.29%; N, 9.72%; Found: C, 64.61%; H, 6.29%; N, 9.73%.

4.1.8.3. (*S*)-*tert*-butyl 6-((*tert*-butoxycarbonyl)amino)-2-(5-oxo-5H-pyrido[3,2-*a*]phenoxazine-10-carboxamido)hexanoate (**3a**). Yield 73%; oil; ¹H NMR (500 MHz, CDCl₃) δ 9.21 (bs, 1H), 9.16–9.15 (dd, *J* = 8.0, 1.6 Hz, 1H), 8.34 (s, 1H), 8.09–8.08 (d, *J* = 8.2 Hz, 1H), 7.86 (m, 1H), 7.44 (d, *J* = 8.2 Hz, 1H), 6.99 (d, *J* = 7.2 Hz, 1H), 6.70 (s, 1H), 4.73–4.69 (m, 1H), 3.14 (m, 2H), 2.03–1.98 (m, 2H), 1.84 (m, 2H), 1.52–1.47 (m, 2H). ¹³C NMR (125 MHz, CDCl₃) δ 184.32, 172.40, 168.61, 165.62, 156.69, 153.86, 147.93, 146.91, 135.30, 134.11, 132.62, 132.11, 131.71, 129.74, 128.13, 127.35, 116.53, 109.63, 82.89, 79.31, 53.20, 41.25, 32.15, 29.56, 29.26, 28.29, 27.95; MS (ESI), *m/z*: 577 (M⁺+1); Anal. Calcd. for C₃₁H₃₆N₄O₇: C, 64.57%; H, 6.29%; N, 9.72%; Found: C, 64.60%; H, 6.30%; N, 9.70%.

4.1.8.4. (*S*)-*tert*-butyl 6-((*tert*-butoxycarbonyl)amino)-2-(5-oxo-5H-pyrido[2,3-*a*]phenoxazine-10-carboxamido)hexanoate (**3'a**). Yield 88%; oil; ¹H NMR (500 MHz, CDCl₃) δ 9.14–9.13 (d, *J* = 2.9 Hz, 1H), 8.59 (d, *J* = 4.7 Hz, 1H), 8.48 (s, 1H), 8.09–8.08 (d, *J* = 8.5 Hz, 1H), 7.72–7.71, 7.71–7.70 (dd, *J* = 7.5, 4.7 Hz, 1H), 7.40–7.38 (d, *J* = 8.5 Hz, 1H), 6.94 (bs, 1H), 6.53 (s, 1H), 4.70–4.67, 4.68–4.66 (dd, *J* = 12.3, 6.8 Hz, 1H), 4.61 (bs, 1H), 3.12 (m, 2H), 1.96 (m, 1H), 1.55 (m, 1H), 1.52–1.45 (m, 2H). ¹³C NMR (125 MHz, CDCl₃) δ 182.33, 171.41, 164.76, 155.85, 153.68, 151.61, 147.42, 146.98, 146.05, 134.22, 132.19, 131.96, 131.50, 129.21, 128.59, 126.30, 116.18, 107.64, 82.45, 78.93, 52.96, 40.08, 32.16, 29.51, 28.25, 27.89, 22.19; MS (ESI), *m/z*: 577

(M⁺+1); Anal. Calcd. for C₃₁H₃₆N₄O₇: C, 64.57%; H, 6.29%; N, 9.72%; Found: C, 64.55%; H, 6.30%; N, 9.70%.

4.1.8.5. (*S*)-*tert*-butyl 2-((*tert*-butoxycarbonyl)amino)-6-(5-oxo-5H-pyrido[3,2-*a*]phenoxazine-10-carboxamido)hexanoate (**4a**). Yield 70%; oil; ¹H NMR (500 MHz, CDCl₃) δ 9.13 (d, *J* = 3.7 Hz, 1H), 9.07–9.05 (d, *J* = 7.8 Hz, 1H), 8.30 (bs, 1H), 8.06–8.04 (d, *J* = 8.3 Hz, 1H), 7.77–7.76, 7.77–7.75 (dd, *J* = 8.1, 4.3 Hz, 1H), 7.42–7.41 (d, *J* = 8.3 Hz, 1H), 6.68 (s, 1H), 6.55 (bs, 1H), 5.16–5.14 (d, *J* = 7.1 Hz, 1H), 4.22 (m, 1H), 3.54 (m, 2H), 1.84 (m, 1H), 1.74 (m, 1H), 1.50–1.44 (m, 2H). ¹³C NMR (125 MHz, CDCl₃) δ 181.09, 172.26, 166.22, 154.03, 154.01, 150.82, 147.32, 145.98, 145.05, 133.42, 132.55, 131.48, 131.45, 129.01, 128.09, 126.55, 116.45, 109.36, 81.86, 79.83, 53.38, 39.74, 32.68, 29.35, 28.38, 27.95, 27.66; MS (ESI), *m/z*: 577 (M⁺+1); Anal. Calcd. for C₃₁H₃₆N₄O₇: C, 64.57%; H, 6.29%; N, 9.72%; Found: C, 64.59%; H, 6.27%; N, 9.69%.

4.1.8.6. (*S*)-*tert*-butyl 2-((*tert*-butoxycarbonyl)amino)-6-(5-oxo-5H-pyrido[2,3-*a*]phenoxazine-10-carboxamido)hexanoate (**4'a**). Yield 85%; oil; ¹H NMR (500 MHz, CDCl₃) δ 9.18–9.17, 9.17–9.16 (dd, *J* = 4.5, 1.6 Hz, 1H), 8.64–8.63, 8.63–8.62 (dd, *J* = 7.9, 1.6 Hz, 1H), 8.44 (bs, 1H), 8.11–8.10, 8.10–8.09 (dd, *J* = 8.5, 2.0 Hz, 1H), 7.76–7.75, 7.75–7.74 (dd, *J* = 7.9, 4.5 Hz, 1H), 7.42–7.40 (d, *J* = 8.5 Hz, 1H), 6.55 (s, 1H), 6.39 (bs, 1H), 5.12–5.10 (d, *J* = 8.0 Hz, 1H), 4.19 (m, 1H), 3.52 (m, 2H), 1.84 (m, 1H), 1.66 (m, 1H), 1.53–1.50 (m, 2H). ¹³C NMR (125 MHz, CDCl₃) δ 182.93, 172.27, 165.83, 162.69, 155.83, 154.11, 152.10, 147.78, 147.43, 146.28, 134.64, 132.53, 132.27, 129.26, 128.96, 126.62, 116.40, 107.79, 81.88, 79.58, 53.41, 39.74, 32.49, 29.33, 28.66, 27.94, 27.65; MS (ESI), *m/z*: 577 (M⁺+1); Anal. Calcd. for C₃₁H₃₆N₄O₇: C, 64.57%; H, 6.29%; N, 9.72%; Found: C, 64.55%; H, 6.28%; N, 9.70%.

4.1.8.7. (*S*)-*tert*-butyl 2-((*tert*-butoxycarbonyl)amino)-6-(5-oxo-5H-pyrido[3,2-*a*]phenoxazine-9-carboxamido)hexanoate (**5a**). Yield 70%; oil; ¹H NMR (400 MHz, CDCl₃) δ 9.06 (d, *J* = 3.1 Hz, 1H), 9.00 (dd, *J* = 8.1, 1.5 Hz, 1H), 7.83 (s, *J* = 8.3 Hz, 1H), 7.78 (m, 2H), 7.72 (m, 1H), 6.87 (bs, 1H), 6.59 (s, 1H), 5.18 (d, *J* = 8.0 Hz, 1H), 4.18 (m, 1H), 3.51 (m, 2H), 1.80 (m, 1H), 1.72 (m, 1H), 1.50–1.44 (m, 2H). ¹³C NMR (125 MHz, CDCl₃) δ 187.32, 172.10, 168.88, 165.12, 156.09, 153.96, 147.90, 146.99, 135.90, 134.67, 133.82, 132.90, 131.51, 129.14, 128.03, 127.55, 117.53, 109.50, 82.99, 79.41, 53.60, 41.15, 32.95, 29.33, 29.30, 28.19, 27.65; MS (ESI), *m/z*: 577 (M⁺+1); Anal. Calcd. for C₃₁H₃₆N₄O₇: C, 64.57%; H, 6.29%; N, 9.72%; Found: C, 64.60%; H, 6.30%; N, 9.69%.

4.1.8.8. (*S*)-*tert*-butyl 2-((*tert*-butoxycarbonyl)amino)-6-(5-oxo-5H-pyrido[2,3-*a*]phenoxazine-9-carboxamido)hexanoate (**5'a**). Yield 90%; oil; ¹H NMR (400 MHz, CDCl₃) δ 9.18 (m, 1H), 8.67 (d, *J* = 7.7 Hz, 1H), 8.10 (m, 1H), 7.83 (s, 1H), 7.80–7.78 (m, 2H), 6.78 (bs, 1H), 6.51 (s, 1H), 5.14 (m, 1H), 4.16 (m, 1H), 3.50 (m, 2H), 1.82–1.69 (m, 6H), 1.49–1.43 (m, 18H). ¹³C NMR (100 MHz, CDCl₃) δ 182.24, 171.71, 165.43, 161.12, 155.54, 153.62, 151.92, 146.95, 143.93, 138.36, 134.44, 131.04, 128.82, 126.40, 123.84, 123.47, 115.16, 107.49, 81.92, 79.28, 53.52, 39.92, 32.82, 28.51, 28.20, 27.90, 22.53; MS (ESI), *m/z*: 577 (M⁺+1); Anal. Calcd. for C₃₁H₃₆N₄O₇: C, 64.57%; H, 6.29%; N, 9.72%; Found: C, 64.60%; H, 6.31%; N, 9.75%.

Step. 2. All the compounds **2a-5a** and **2'a-5'a** (0.54 mmol) were dissolved in formic acid (31 mL) and the solutions, stirred for 72 h at room temperature, were evaporated under reduced pressure. The crude products were purified by Flow Lab semi-preparative HPLC System on a Phenomenex Axia Packed Luna C18(2) column (50 \times 21.20 mm, 5 μ m, 100 Å) using CH₃CN:H₂O:TFA (80:20:0.1) as eluent with a flow rate of 12 mL/min.

4.1.8.9. (*S*)-6-amino-2-(5-oxo-5*H*-pyrido[3,2-*a*]phenoxazine-9-carboxamido)hexanoic acid (**2**). Yield 88%; ^1H NMR (400 MHz, CD₃OD) δ 9.29–9.30 (d, $J = 7.2$ Hz, 1H), 9.09 (bs, 1H), 8.07–8.04 (d, 2H), 7.97 (m, 2H), 6.70 (s, 1H), 4.65 (m, 1H), 2.97 (m, 2H), 2.10 (m, 1H), 1.94 (m, 1H), 1.75 (m, 2H), 1.51 (m, 2H). ^{13}C NMR (100 MHz, CD₃OD) δ 187.40, 186.04, 170.84, 156.92, 154.97, 150.25, 148.00, 146.24, 140.61, 140.10, 132.37, 128.99, 126.16, 124.18, 122.80, 115.63, 108.13, 56.04, 41.66, 37.69, 33.73, 24.63; MS (ESI), m/z : 421 ($\text{M}^+ + 1$); Anal. Calcd. for C₂₂H₂₀N₄O₅: C, 62.85%; H, 4.79%; N, 13.33%; Found: C, 62.83%; H, 4.80%; N, 13.28%.

4.1.8.10. (*S*)-6-amino-2-(5-oxo-5*H*-pyrido[3,2-*a*]phenoxazine-10-carboxamido)hexanoic acid (**3**). Yield 85%; oil; ^1H NMR (400 MHz, CD₃OD) δ 9.42 (d, $J = 7.0$ Hz, 1H), 9.10 (m, 1H), 8.46 (s, 1H), 8.15 (m, 2H), 7.59–7.57 (d, $J = 8.5$ Hz, 1H), 6.71 (s, 1H), 4.67 (m, 1H), 2.92 (m, 2H), 2.04 (m, 1H), 1.85 (m, 1H), 1.75 (m, 2H), 1.68 (m, 2H). ^{13}C NMR (125 MHz, CD₃OD) δ 186.42, 175.00, 165.62, 156.66, 155.86, 147.83, 147.01, 139.30, 138.11, 137.12, 132.01, 130.61, 129.44, 125.73, 125.55, 118.13, 109.53, 56.20, 41.35, 32.85, 31.16, 24.85; MS (ESI), m/z : 421 ($\text{M}^+ + 1$); Anal. Calcd. for C₂₂H₂₀N₄O₅: C, 62.85%; H, 4.79%; N, 13.33%; Found: C, 62.91%; H, 4.80%; N, 13.35%.

4.1.8.11. (*S*)-2-amino-6-(5-oxo-5*H*-pyrido[3,2-*a*]phenoxazine-10-carboxamido)hexanoic acid (**4**). Yield 94%; oil; ^1H NMR (400 MHz, CD₃OD) δ 9.26–9.24 (dd, $J = 7.5, 4.0$ Hz, 1H), 9.06 (bs, 1H), 8.40–8.39 (d, $J = 2.0$ Hz, 1H), 8.10–8.08 (dd, $J = 8.6, 2.0$ Hz, 1H), 7.56–7.54 (d, $J = 8.6$ Hz, 1H), 6.67 (s, 1H), 3.98 (m, 1H), 3.46–3.45 (m, 2H), 2.01 (m, 2H), 1.92 (m, 1H), 1.75 (m, 2H), 1.56 (m, 1H). ^{13}C NMR (100 MHz, CD₃OD) δ 187.49, 176.90, 165.67, 156.00, 155.86, 147.80, 147.38, 139.99, 138.99, 138.42, 132.71, 131.50, 130.01, 129.04, 127.31, 116.13, 107.10, 52.34, 39.05, 29.44, 28.46, 22.15; MS (ESI), m/z : 421 ($\text{M}^+ + 1$); Anal. Calcd. for C₂₂H₂₀N₄O₅: C, 62.85%; H, 4.79%; N, 13.33%; Found: C, 62.90%; H, 4.81%; N, 13.34%.

4.1.8.12. (*S*)-2-amino-6-(5-oxo-5*H*-pyrido[3,2-*a*]phenoxazine-9-carboxamido)hexanoic acid (**5**). Yield 95%; oil; ^1H NMR (400 MHz, CD₃OD) δ 9.28–9.26 (dd, $J = 8.0, 4.0$ Hz, 1H), 9.07 (m, 1H), 8.03–8.01 (m, 2H), 7.90–7.88 (m, 2H), 6.68 (s, 1H), 4.01 (t, $J = 5.9$ Hz, 1H), 3.47–3.45 (m, 2H), 2.04–1.97 (m, 3H), 1.75 (m, 2H), 1.61 (m, 1H). ^{13}C NMR (125 MHz, CD₃OD) δ 187.42, 176.40, 165.82, 156.66, 155.96, 147.80, 147.31, 139.49, 138.91, 138.12, 133.01, 130.21, 129.04, 125.63, 125.50, 118.14, 109.55, 56.00, 41.45, 32.88, 31.06, 24.95; MS (ESI), m/z : 421 ($\text{M}^+ + 1$); Anal. Calcd. for C₂₂H₂₀N₄O₅: C, 62.85%; H, 4.79%; N, 13.33%; Found: C, 62.81%; H, 4.77%; N, 13.31%.

4.1.8.13. (*S*)-6-amino-2-(5-oxo-5*H*-pyrido[2,3-*a*]phenoxazine-9-carboxamido)hexanoic acid (**2'**). Yield 85%; ^1H NMR (400 MHz, CD₃OD) δ 9.09–9.08 (d, $J = 3.1$ Hz, 1H), 8.63–8.61 (dd, $J = 8.0, 4.0$ Hz, 1H), 8.06–8.05 (d, $J = 8.0$ Hz, 1H), 7.96–7.84 (m, 3H), 6.50 (s, 1H), 4.57 (m, 1H), 2.95 (m, 2H), 2.02 (m, 1H), 1.85 (m, 1H), 1.57 (m, 2H), 1.52 (m, 2H). ^{13}C NMR (100 MHz, CD₃OD) δ 185.60, 179.24, 169.03, 156.09, 150.58, 149.78, 140.87, 137.45, 137.17, 133.01, 131.62, 130.71, 129.74, 120.21, 118.04, 113.59, 109.46, 42.04, 34.30, 32.34, 29.64, 25.32; MS (ESI), m/z : 421 ($\text{M}^+ + 1$); Anal. Calcd. for C₂₂H₂₀N₄O₅: C, 62.85%; H, 4.79%; N, 13.33%; Found: C, 62.90%; H, 4.81%; N, 13.34%.

4.1.8.14. (*S*)-6-amino-2-(5-oxo-5*H*-pyrido[2,3-*a*]phenoxazine-10-carboxamido)hexanoic acid (**3'**). Yield 83%; oil; ^1H NMR (500 MHz, CD₃OD) δ 9.07 (bs, 1H), 8.59 (d, $J = 8.0$ Hz, 1H), 8.41 (d, $J = 8.0$ Hz, 1H), 8.10 (d, $J = 8.0$ Hz, 1H), 7.85 (m, 1H), 7.49 (d, $J = 7.9$ Hz, 1H), 6.50 (s, 1H), 4.63 (m, 1H), 2.85 (m, 2H), 2.12 (m, 1H), 1.94 (m, 1H), 1.76 (m, 2H), 1.61 (m, 2H). ^{13}C NMR (125 MHz, CD₃OD) δ 184.84, 168.93, 155.31, 154.35, 149.31, 148.53, 136.20, 134.58, 134.17, 133.77, 133.31, 132.14, 131.08, 130.60, 128.80, 118.06, 108.65, 54.80, 41.15, 32.65,

28.65, 24.75; MS (ESI), m/z : 421 ($\text{M}^+ + 1$); Anal. Calcd. for C₂₂H₂₀N₄O₅: C, 62.85%; H, 4.79%; N, 13.33%; Found: C, 62.90%; H, 4.81%; N, 13.31%.

4.1.8.15. (*S*)-2-amino-6-(5-oxo-5*H*-pyrido[2,3-*a*]phenoxazine-10-carboxamido)hexanoic acid (**4'**). Yield 83%; oil; ^1H NMR (500 MHz, CD₃OD) δ 9.08 (bs, 1H), 8.62–8.60 (d, $J = 8.0$ Hz, 1H), 8.39 (d, $J = 4.0$ Hz, 1H), 8.08–8.06 (d, $J = 7.1$ Hz, 1H), 7.86 (s, 1H), 7.51–7.49 (d, $J = 7.9$ Hz, 1H), 6.50 (s, 1H), 3.68 (s, 1H), 3.42 (m, 2H), 1.83 (m, 2H), 1.70 (m, 2H), 1.48 (m, 2H). ^{13}C NMR (125 MHz, CD₃OD) δ 186.27, 177.01, 165.07, 155.89, 154.75, 148.20, 146.98, 142.90, 137.99, 137.53, 129.97, 128.87, 124.55, 124.01, 122.35, 119.08, 109.77, 55.61, 38.97, 33.20, 26.52, 22.44; MS (ESI), m/z : 421 ($\text{M}^+ + 1$); Anal. Calcd. for C₂₂H₂₀N₄O₅: C, 62.85%; H, 4.79%; N, 13.33%; Found: C, 62.90%; H, 4.81%; N, 13.33%.

4.1.8.16. (*S*)-2-amino-6-(5-oxo-5*H*-pyrido[2,3-*a*]phenoxazine-9-carboxamido)hexanoic acid (**5'**). Yield 93%; oil; ^1H NMR (500 MHz, CD₃OD) δ 9.06–9.05 (dd, $J = 4.2, 1.2$ Hz, 1H), 8.63 (dd, $J = 6.1, 1.2$ Hz, 1H), 8.01–8.00 (m, 2H), 7.91–7.87 (m, 2H), 6.51 (s, 1H), 3.52 (m, 1H), 3.39 (m, 2H), 1.83 (m, 2H), 1.56 (m, 1H), 1.36 (m, 3H). ^{13}C NMR (125 MHz, CD₃OD) δ 186.26, 177.40, 165.50, 156.00, 154.72, 148.89, 147.50, 141.00, 139.50, 138.20, 133.01, 128.28, 125.11, 124.50, 119.85, 118.00, 108.01, 53.60, 39.45, 33.22, 26.88, 22.03; MS (ESI), m/z : 421 ($\text{M}^+ + 1$); Anal. Calcd. for C₂₂H₂₀N₄O₅: C, 62.85%; H, 4.79%; N, 13.33%; Found: C, 62.88%; H, 4.80%; N, 13.35%.

4.2. Chemicals, DNAs, and proteins

AMSA, VP-16, Doxo and AMD were purchased from Sigma-Aldrich (Milan, Italy). Negatively supercoiled plasmid pBR322 DNA was purchased from New England Biolabs (Beverly, MA, USA). Relaxed plasmid DNA was prepared by incubating negatively supercoiled pBR322 DNA with human Topo I, which was purchased from Topogen (Port Orange, FL, USA). The α form of human Topo II was purchased from both Topogen. Purified human Topo II α and II β were purchased from LAE Biotech International.

4.2.1. Cells

Test compounds were dissolved in DMSO at an initial concentration of 200 μM and were then serially diluted in culture medium. Cell lines were from American type Culture Collection (ATCC). Leukemia- and lymphoma-derived cells were grown in Roswell Park Memorial Institute (RPMI) 1640 containing 10% fetal calf serum (FCS), 100 U/mL penicillin G, and 100 $\mu\text{g}/\text{mL}$ streptomycin. Solid-tumor-derived cells were grown in their specific media supplemented with 10% FCS and antibiotics. Cell cultures were incubated at 37 $^{\circ}\text{C}$ in a humidified 5% CO₂ atmosphere. Cell cultures were periodically checked for the absence of mycoplasma contamination by the Hoechst staining method.

4.2.2. Antiproliferative assays

Exponentially growing leukemia and lymphoma cells were resuspended at a density of 1×10^5 cells/mL in RPMI containing serial dilutions of the test drugs. Cell viability was determined after 96 h at 37 $^{\circ}\text{C}$ by the 3-(4,5-dimethylthiazol-2-yl)-2,5-diphenyltetrazolium bromide (MTT) method. The activity against solid-tumor-derived cells was evaluated in exponentially growing cultures seeded at 5×10^4 cells/mL and allowed to adhere for 16 h to culture plates before the addition of drugs. Cell viability was determined by the MTT method 4 days later.

4.2.3. Linear regression analysis

Tumor cell growth at each drug concentration was expressed as the percentage of untreated controls, and the concentration

resulting in 50% (IC₅₀) growth inhibition was determined by linear regression analysis.

4.3. UV–visible spectral measurements

The UV–Visible spectra of free DNA and its complexes with compound **5** were recorded on PerkinElmer 550S spectrometer. Quartz cuvette with a path length of 1 cm was employed for the examination. DNA solution of 0.2 mM concentration was used with varying concentration of drug (1×10^{-1} to 3×10^{-2} mM). Binding constant for the complexation between **5** and DNA was determined using the method described by Kanakis et al. [69]. Calculated binding constant depends on the supposition that only one kind of interaction occurs between DNA (D) and **5** (M) in aqueous solution forming one kind of complex (DM). It is also supposed that the substrate and the ligand obey Beer-Lambert's law for the absorbance of light. The absorbance of DNA solution (A₀) at its total concentration (D_t) with a path length (l) of 1 cm is:

$$A_0 = \epsilon_D l D_t \quad (1)$$

where ϵ_D is the molar absorptivity of free DNA. The absorbance of solution (A_M), including the total concentration of DNA (D_t) along with the total concentration of **5** (M_t), is:

$$A_M \rightarrow \epsilon_D l [D] + \epsilon_M l [M] + \epsilon_{DM} l [DM] \quad (2)$$

where [D] is the concentration of uncomplexed DNA, [M] is the concentration of uncomplexed **5**, [DM] is the concentration of **5**–DNA complex, ϵ_M is the molar absorptivity of **5** and ϵ_{DM} is the molar absorptivity of **5**–DNA complex. After combining with the mass balance of DNA and **5**, the absorbance equation can be written as:

$$A_M \rightarrow \epsilon_D l D_t + \epsilon_M l M_t + \Delta \epsilon_{DM} l [DM] \quad (3)$$

$$\Delta \epsilon_{DM} \rightarrow \epsilon_{DM} - \epsilon_D - \epsilon_M$$

The absorbance of solution (A) measured against the total concentration of **5** as reference is

$$A \rightarrow \epsilon_D l D_t + \Delta \epsilon_{DM} l [DM] \quad (4)$$

The stability constant (K_{DM}) for the formation of the complex (DM) can be given as:

$$K_{DM} \rightarrow [DM] / ([D][M]) \quad (5)$$

Combining Eqs. (4) and (5)

$$\Delta A \rightarrow K_{DM} \Delta \epsilon_{DM} l [D][M] \quad (6)$$

$$\Delta A = A - A_0$$

From the mass balance equation $D_t = [D] + [DM]$, we get $[D] = D_t / (1 + K_{DM}[M])$, which gives

$$\frac{\Delta A}{l} \rightarrow \frac{D_t K_{DM} \Delta \epsilon_{DM} [M]}{1 + K_{DM} [M]} \quad (7)$$

There is a hyperbolic relation between the free drug molecule concentration and its interaction with DNA. Linear transformation of Eq. (6) is obtained by taking the reciprocal of both side of Eq. (7) that gives:

$$\frac{l}{\Delta A} \rightarrow \frac{1}{D_t K_{DM} \Delta \epsilon_{DM} [M]} + \frac{1}{D_t \Delta \epsilon_{DM}} \quad (8)$$

The double reciprocal plot of 1/DA vs. 1/[M] is linear and the binding constant (K) can be estimated by computing the ratio of the intercept to the slope.

4.4. DNA unwinding assay

A DNA intercalation assay was performed as described previously [52]. Briefly, reaction mixtures (20 μl) containing 50 mM Tris-HCl (pH 7.5 at 23 °C), 2.5 mM MgCl₂, 0.5 mM dithiothreitol (DTT), 50 μg/mL bovine serum albumin (BSA), 300 ng of relaxed plasmid DNA, and 2 units of human Topo I (Topogen, Port Orange, FL) were incubated at 37 °C for 10 min in the absence or presence of the indicated concentrations of the various compounds. Reactions were terminated by extraction with phenol/chloroform/isoamyl alcohol (25:24:1, v/v) and the DNA products were analyzed by electrophoresis through vertical 1.2% SeaKem ME agarose (Lonza, Rockland, ME) gels (14 × 10 × 0.3 cm) at 2 V/cm for 15 h in TAE buffer [50 mM Tris-HCl (pH 7.9 at 23 °C), 40 mM sodium acetate and 1 mM EDTA]. Gels were stained with EtBr and photographed using a Stratagene Eagle Eye gel documentation system (Agilent Technologies, Santa Clara, CA).

4.5. Computational chemistry

4.5.1. Ligand, DNA and protein setup

The 3D structures of **2–5** were generated with the Maestro Build Panel implemented in Maestro 11.1 (Schrödinger, LLC, New York, NY, 2018) software package, and their protonation state at physiological pH 7.4 was assigned using Epik 4.0 (Schrödinger, LLC, New York, NY, 2018). The X-ray coordinates of d(GAAGCTTC)₂ octamer complexed with AMD (PDB code = 209D) [56] and human Topo II α in complex with DNA and etoposide (PDB code = 5GWK) [63] were extracted from the Protein Data Bank [70]. The structures were then prepared using the Protein Preparation Wizard of the Schrödinger graphical interface Maestro. Water molecules and co-crystallized ligands were removed, hydrogen atoms were added and the central intercalation site was utilized for docking experiments.

4.5.2. Molecular docking

AutoDock 4.2 software package [53] was employed for docking simulations. Ligand, DNA and protein structures were converted to AD4 format files using the graphical user interface AutoDockTools (ADT); the Gasteiger–Marsili partial charges and Kollman charges were then assigned to the ligand and nucleic acid atoms, respectively. The grid box was centered on the intercalation site in case of DNA and on the etoposide binding site in case of Topo II α , allowing the ligand to explore the whole conformational space. Thus, grid points of 60 × 60 × 60 with a 0.375 Å spacing were calculated around the docking area for all the ligand atom types using AutoGrid 4.2. A total of 200 separate docking calculations were executed for each ligand. Each docking run consisted of 25 million energy evaluations using the Lamarckian genetic algorithm local search method. Otherwise default docking parameters were applied. Docking conformations were clustered on the basis of the root mean square deviation (rmsd) between the Cartesian coordinates of the ligand atoms (cutoff = 0.8 Å) and were ranked based on the AutoDock scoring function [71].

With the purpose to check the reliability of the above reported docking protocol, docking validation was performed using a simplified model of AMD, consisting of the phenoxazone ring with the two cyclic depsipeptides replaced by methylamide groups. We obtained an almost perfect match between the simplified AMD model and the crystallized conformation of the phenoxazone ring of AMD, with a RMSD value of 0.80 Å (Fig. S18 in Supplementary data). Therefore, this methodology was consistently used to

perform all the docking experiments within the study. Figures were generated with Pymol 2.0 (Schrödinger, LLC, New York, NY, 2018).

4.5.3. Quantum mechanics calculations

All calculations were performed with Jaguar 9.0 (Schrödinger, LLC, New York, NY, 2017). The structures of pyridophenoxazinones (where the carboxamide side chains at 9 and 10 positions were replaced with methylamide groups), and C–G and G–C base pairs (where the deoxyribose rings were replaced with methyl groups) were optimized at the HF/6-31G** level of theory. The single point energy calculations were performed at the LMP2/6-31G* and HF/6-31G* levels of theory. The NBO analysis [72] was performed at the HF/6-31G** level of theory. The interaction between filled orbitals of one subsystem and vacant orbitals of another subsystem can be used as a measure of the intermolecular delocalization, as it represents a deviation of the complex from the Lewis structure. The hyperconjugative interaction energy can be deduced from the second-order perturbation approach. This type of interaction is also called charge transfer energy, though the electron density transferred between subsystems is relatively small but chemically significant. It has been estimated that 0.001e of charge transfer roughly corresponds to 1 kcal/mol of the stabilization energy [73]. Here, we use

$$E_{CT} = \Sigma E(2) \quad (1)$$

where E(2) is all of the individual intermolecular second-order hyperconjugative interactions between the ligand and the neighboring DNA base pairs that exceed a default threshold of 0.05 kcal/mol calculated from NBO analysis at the HF/6-31G** level of theory, reflecting the major contribution of charge transfer to the stabilization of the drug-DNA complex.

4.6. Relaxation assay of human Topo II α

The reaction mixture contained 20 mM Tris-HCl, pH 7.5, 7.5 mM MgCl₂, 0.5 mM DTT, 150 mM KCl, 1 mM ATP, and 200 ng of pBR322 DNA. The reaction was initiated by the addition of DNA Topo II α and allowed to proceed at 30 °C for 15 min. Reactions were terminated by the addition of loading buffer (0.1% SDS, 0.05% bromophenol blue, 2.5 mM EDTA, and 10% sucrose, final concentrations). The samples were electrophoresed in 1.2% agarose gels at 0.5 V/cm for 18 h in TBE buffer (90 mM Tris-borate, and 1 mM EDTA, pH 8). Gels were stained with 0.5 μ g/mL EtBr to visualize DNA and were photographed under UV illumination as described previously [74].

4.7. Formation of Topo II α and Topo II β cleavable complexes in vitro

The experimental conditions were the same as for the relaxation assay except that approximately 50-fold more DNA Topo II α and Topo II β was used. The reaction was initiated with the addition of the enzymes. After 10 min at 30 °C, the reactions were terminated by adding 0.35% SDS and 0.3 mg/mL proteinase K (final concentrations) followed by incubation at 56 °C for 1 h. The DNA cleavage products were separated by electrophoresis in 1.2% agarose gels containing EtBr (0.5 μ g/mL) at 1 V/cm for 18 h in TBE (Tris-borate-EDTA) buffer and were visualized and photographed under UV illumination as described previously [74].

4.8. Comet assay

Comet assay was performed according to protocol by Tice et al. [75]. Approximately 1×10^5 MCF-7 cells were seeded in 24-well tissue-culture plates and after 24 h treated with increasing concentration of **5** and 10 μ M VP-16 (positive control) for 24 h. Cells

were harvested by trypsinization, washed with phosphate buffered saline (PBS) and resuspended in ice-cold PBS. All steps were performed at room temperature under dimmed or yellow light to prevent DNA damage unless otherwise specified. About 25 μ l of the resuspended cells was mixed with 75 μ l 0.5% low-melting agarose at 37 °C and spread uniformly with the side of a microtip on pre-heated (37 °C) microscopic slides. The slides were placed at 4 °C in the dark until gelling occurred and then immersed in prechilled lysis solution (10 mM Tris, 100 mM EDTA, 2.5 M NaCl, 1% Triton X100, 10% DMSO and pH 10.0) at 4 °C. After 1 h of incubation, the buffer was drained from slides and immersed in freshly prepared alkaline-unwinding solution (300 mM NaOH, 1 mM EDTA and pH 13.0) at room temperature for 30–60 min. After lysis and unwinding, the slides were placed in a horizontal electrophoresis tank filled with freshly prepared alkaline electrophoresis buffer, and electrophoresis was carried out at 30 V for 15 min. After electrophoresis, the slides were covered with neutralization buffer (0.4 M Tris HCl and pH 7.5) for 5 min and washed twice by immersing in distilled water for 5 min each, then in 70% ethanol for 10 min. Thereafter, the slides were dried at room temperature for overnight or at 45 °C for 10–15 min, then stained with PI for 10 min in dark at 4 °C. DNA migration was observed using fluorescence microscope (Nikon, Japan) at a magnification of 10 \times . The comet tail lengths were analyzed by TriTek CometScore™ software. Data were represented both by imaging and graphically by randomly selecting comet lengths of MCF-7 cells.

4.9. Western blot analysis

Mcf-7 cells were collected after treatment with **5** for 0.5, 1 and 3 h and washed three times with ice-cold PBS. For nucleus protein isolation, cells were lysed with radio-immunoprecipitation assay (RIPA) lysis buffer (50 mM Tris-HCl at pH 7.5, 150 mM NaCl, 1% Triton X-100, 10% deoxycholate, 0.1% SDS, 0.1% phenylmethylsulfonyl fluoride (PMSF) and proteinase inhibitor cocktails). Equivalent amounts of proteins were resolved by SDS-PAGE and transferred to poly(vinylidene fluoride) (PVDF) membranes (Bio-Rad, CA, USA). Antibodies corresponding to the proteins were used. β -actin was used as the loading control. Proteins were visualized with a horse radish peroxidase-conjugated secondary antibody using an enhanced chemiluminescence kit (Visual Protein, Taiwan) for detection.

Notes

The authors declare no competing financial interest.

Declaration of competing interest

The authors declare that they have no known competing financial interests or personal relationships that could have appeared to influence the work reported in this paper.

Acknowledgments

This study was financially supported by grants “Combattere la resistenza tumorale: piattaforma integrata multidisciplinare per un approccio tecnologico innovativo alle oncoterapie “CAMPANIA ONCOTERAPIE” (project no. B61G18000470007) of Regione Campania (Italy) (A. L.). The authors would like to thank the Centro Interdipartimentale di Metodologie Chimico-Fisiche CIMCF and the Centro Interdipartimentale di Analisi Strumentale dell’University of Naples Federico II. We would like to thank Dr. Giorgia Oliviero for synthesizing the oligonucleotide d[(GAAGCTTC)]₂ used in this work.

Appendix A. Supplementary data

Supplementary data to this article can be found online at <https://doi.org/10.1016/j.ejmech.2019.111960>.

References

- [1] A. Rescifina, C. Zagni, M.G. Varrica, V. Pistarà, A. Corsaro, Recent advances in small organic molecules as DNA intercalating agents: synthesis, activity, and modeling, *Eur. J. Med. Chem.* 74 (2014) 95–115.
- [2] A. Bolognese, G. Correale, M. Manfra, A. Lavecchia, O. Mazzoni, E. Novellino, V. Barone, A. Pani, E. Tramontano, P. La Colla, C. Murgioni, I. Serra, G. Setzu, R. Loddo, Antitumor agents. 1. Synthesis, biological evaluation, and molecular modeling of 5H-pyrido[3,2-a]phenoxazin-5-one, a compound with potent antiproliferative activity, *J. Med. Chem.* 45 (2002) 5205–5216.
- [3] A. Bolognese, G. Correale, M. Manfra, A. Lavecchia, O. Mazzoni, E. Novellino, V. Barone, P. La Colla, R. Loddo, Antitumor agents. 2. Synthesis, structure-activity relationships, and biological evaluation of substituted 5H-pyrido[3,2-a]phenoxazin-5-ones with potent antiproliferative activity, *J. Med. Chem.* 45 (2002) 5217–5223.
- [4] A. Bolognese, G. Correale, M. Manfra, A. Lavecchia, E. Novellino, S. Pepe, Antitumor agents. 5. Synthesis, structure-activity relationships, and biological evaluation of dimethyl-5H-pyrido[3,2-a]phenoxazin-5-ones, tetrahydro-5h-benzopyridophenoxazin-5-ones, and 5h-benzopyridophenoxazin-5-ones with potent antiproliferative activity, *J. Med. Chem.* 49 (2006) 5110–5118.
- [5] A. Alberti, A. Bolognese, M. Guerra, A. Lavecchia, D. Macciantelli, M. Marcaccio, E. Novellino, F. Paolucci, Antitumor agents 4. Characterization of free radicals produced during reduction of the antitumor drug 5H-pyrido[3,2-a]phenoxazin-5-one: an EPR study, *Biochemistry* 42 (2003) 11924–11931.
- [6] C. Bailly, Contemporary challenges in the design of topoisomerase II inhibitors for cancer chemotherapy, *Chem. Rev.* 112 (2012) 3611–3640.
- [7] J.L. Nitiss, Targeting DNA topoisomerase II in cancer chemotherapy, *Nat. Rev. Cancer* 9 (2009) 338–350.
- [8] S.M. Vos, E.M. Tretter, B.H. Schmidt, J.M. Berger, All tangled up: how cells direct, manage and exploit topoisomerase function, *Nat. Rev. Mol. Cell Biol.* 12 (2011) 827–841.
- [9] S.M. Cuya, M.A. Bjornsti, R. van Waardenburg, DNA topoisomerase-targeting chemotherapeutics: what's new? *Cancer Chemother. Pharmacol.* 80 (2017) 1–14.
- [10] Y. Pommier, E. Leo, H. Zhang, C. Marchand, DNA topoisomerases and their poisoning by anticancer and antibacterial drugs, *Chem. Biol.* 17 (2010) 421–433.
- [11] Y. Pommier, P. Pourquier, Y. Fan, D. Strumberg, Mechanism of action of eukaryotic DNA topoisomerase I and drugs targeted to the enzyme, *Biochim. Biophys. Acta* 1400 (1998) 83–105.
- [12] D.A. Burden, N. Osheroff, Mechanism of action of eukaryotic topoisomerase II and drugs targeted to the enzyme, *Biochim. Biophys. Acta* 1400 (1998) 139–154.
- [13] A.M. Azarova, Y.L. Lyu, C.-P. Lin, Y.-C. Tsai, J.Y.-N. Lau, J.C. Wang, L.F. Liu, Roles of DNA topoisomerase II isozymes in chemotherapy and secondary malignancies, *Proc. Natl. Acad. Sci. U. S. A.* 104 (2007) 11014–11019.
- [14] E. Toyoda, S. Kagaya, I.G. Cowell, A. Kurosawa, K. Kamoshita, K. Nishikawa, S. Iizumi, H. Koyama, C.A. Austin, N. Adachi, NK314, a topoisomerase II inhibitor that specifically targets the α isoform, *J. Biol. Chem.* 283 (2008) 23711–23720.
- [15] A.K. Larsen, A. Skladanowski, Cellular resistance to topoisomerase-targeted drugs: from drug uptake to cell death, *Biochim. Biophys. Acta* 1400 (1998) 257–274.
- [16] R. Ishida, T. Miki, T. Narita, R. Yui, M. Sato, K.R. Utsumi, K. Tanabe, T. Andoh, Inhibition of intracellular topoisomerase II by antitumor bis(2,6-dioxopiperazine) derivatives: mode of cell growth inhibition distinct from that of cleavable complex-forming type inhibitors, *Cancer Res.* 51 (1991) 4909–4916.
- [17] Y. Onishi, Y. Azuma, H. Kizaki, bis(2,6-dioxopiperazine) derivatives, topoisomerase II inhibitors which do not form a DNA cleavable complex, induce thymocyte apoptosis, *Biochem. Mol. Biol. Int.* 32 (1994) 115–122.
- [18] B.B. Hasinoff, T.I. Kuschak, J.C. Yalowich, A.M. Creighton, A QSAR study comparing the cytotoxicity and DNA topoisomerase II inhibitory effects of bisdioxopiperazine analogs of ICRF-187 (dexrazoxane), *Biochem. Pharmacol.* 50 (1995) 953–958.
- [19] J.L. Nitiss, DNA topoisomerase II and its growing repertoire of biological functions, *Nat. Rev. Cancer* 9 (2009) 327–337.
- [20] P. Furet, J. Schoepfer, T. Radimerski, P. Chene, Discovery of a new class of catalytic topoisomerase II inhibitors targeting the ATP-binding site by structure based design. Part I, *Bioorg. Med. Chem. Lett.* 19 (2009) 4014–4017.
- [21] K.Y. Jun, E.Y. Lee, M.J. Jung, O.H. Lee, E.S. Lee, H.Y. Park, Choo, Y. Na, Y. Kwon, Synthesis, biological evaluation, and molecular docking study of 3-(3'-heteroatom substituted-2'-hydroxy-1'-propyloxy) xanthone analogues as novel topoisomerase II catalytic inhibitor, *Eur. J. Med. Chem.* 46 (2011) 1964–1971.
- [22] W. Hu, X.-S. Huang, J.-F. Wu, L. Yang, Y.-T. Zheng, Y.-M. Shen, Z.-Y. Li, X. Li, Discovery of novel topoisomerase II inhibitors by medicinal chemistry approaches, *J. Med. Chem.* 61 (2018) 8947–8980.
- [23] S.B. Neidle, Ch, J.P. Henichart, Molecular pharmacology of Intercalator–Groove binder hybrid molecules, in: *Molecular Aspects of Anticancer Drug DNA Interactions*, Taylor & Francis Group, Oxon, U.K., 1994.
- [24] M. Masquelier, R. Baurain, A. Trouet, Amino acid and dipeptide derivatives of daunorubicin. 1. Synthesis, physicochemical properties, and lysosomal digestion, *J. Med. Chem.* 23 (1980) 1166–1170.
- [25] K. Breistol, H.R. Hendriks, D.P. Berger, S.P. Langdon, H.H. Fiebig, O. Fodstad, The antitumor activity of the prodrug N-L-leucyl-doxorubicin and its parent compound doxorubicin in human tumour xenografts, *Eur. J. Cancer* 34 (1998) 1602–1606.
- [26] Y. van Hensbergen, H.J. Broxterman, Y.W. Elderkamp, J. Lankelma, J.C. Beers, M. Heijn, E. Boven, K. Hoekman, H.M. Pinedo, A doxorubicin-CNGRC-peptide conjugate with prodrug properties, *Biochem. Pharmacol.* 63 (2002) 897–908.
- [27] C. Ryppa, H. Mann-Steinberg, M.L. Biniossek, R. Satchi-Fainaro, F. Kratz, In vitro and in vivo evaluation of a paclitaxel conjugate with the divalent peptide E-[c(RGDfK)2] that targets integrin α v β 3, *Int. J. Pharm.* 368 (2009) 89–97.
- [28] C.J. Hsiao, T.K. Li, Y.L. Chan, L.W. Hsin, C.H. Liao, C.H. Lee, P.C. Lyu, J.H. Guh, WRC-213, an L-methionine-conjugated mitoxantrone derivative, displays anticancer activity with reduced cardiotoxicity and drug resistance: identification of topoisomerase II inhibition and apoptotic machinery in prostate cancers, *Biochem. Pharmacol.* 75 (2008) 847–856.
- [29] D. Ravel, V. Dubois, J. Quinonero, F. Meyer-Losic, J. Delord, P. Rochaix, C. Nicolazzi, F. Ribes, C. Mazerolles, E. Assouly, K. Vialatte, I. Hor, J. Kearsley, A. Trouet, Preclinical toxicity, toxicokinetics, and antitumoral efficacy studies of DTS-201, a tumor-selective peptidic prodrug of doxorubicin, *Clin. Cancer Res.* 14 (2008) 1258–1265.
- [30] S. Zitzmann, V. Ehemann, M. Schwab, Arginine-glycine-aspartic acid (RGD)-peptide binds to both tumor and tumor-endothelial cells in vivo, *Cancer Res.* 62 (2002) 5139–5143.
- [31] W. Arap, R. Pasqualini, E. Ruoslahti, Cancer treatment by targeted drug delivery to tumor vasculature in a mouse model, *Science* 279 (1998) 377–380.
- [32] C. Monneret, Recent developments in the field of antitumor anthracyclines, *Eur. J. Med. Chem.* 36 (2001) 483–493.
- [33] F.M. de Groot, H.J. Broxterman, H.P. Adams, A. van Vliet, G.I. Tesser, Y.W. Elderkamp, A.J. Schraa, R.J. Kok, G. Molema, H.M. Pinedo, H.W. Scheeren, Design, synthesis, and biological evaluation of a dual tumor-specific motif containing integrin-targeted plasmin-cleavable doxorubicin prodrug, *Mol. Cancer Ther.* 1 (2002) 901–911.
- [34] X. Bu, L.W. Deady, G.J. Finlay, B.C. Baguley, W.A. Denny, Synthesis and cytotoxic activity of 7-oxo-7H-dibenz[f,i]isoquinoline and 7-oxo-7H-benzo[e]perimidine derivatives, *J. Med. Chem.* 44 (2001) 2004–2014.
- [35] K. Tkaczyk-Gobis, J. Tarasiuk, O. Seksek, B. Stefanska, E. Borowski, A. Garnier-Suillerot, Transport of new non-cross-resistant antitumor compounds of the benzoperimidine family in multidrug resistant cells, *Eur. J. Pharmacol.* 413 (2001) 131–141.
- [36] P. De Isabella, F. Zunino, G. Capranico, Base sequence determinants of amonafide stimulation of topoisomerase II DNA cleavage, *Nucleic Acids Res.* 23 (1995) 223–229.
- [37] C. Bailly, Topoisomerase I poisons and suppressors as anticancer drugs, *Curr. Med. Chem.* 7 (2000) 39–58.
- [38] S. Fujimoto, Promising antitumor activity of a novel quinoline derivative, TAS-103, against fresh clinical specimens of eight types of tumors measured by flow cytometric DNA analysis, *Biol. Pharm. Bull.* 30 (2007) 1923–1929.
- [39] L.P. Wakelin, A. Adams, W.A. Denny, Kinetic studies of the binding of acridinecarboxamide topoisomerase poisons to DNA: implications for mode of binding of ligands with uncharged chromophores, *J. Med. Chem.* 45 (2002) 894–901.
- [40] F. Malonne, S. Farinelle, C. Decaestecker, L. Gordower, J. Fontaine, F. Chaminaud, J.M. Saucier, G. Atassi, R. Kiss, In vitro and in vivo pharmacological characterizations of the antitumor properties of two new olivacine derivatives, S16020-2 and S30972-1, *Clin. Cancer Res.* 6 (2000) 3774–3782.
- [41] H. Ihmels, D. Otto, Intercalation of organic dye molecules into double-stranded DNA—general principles and recent developments, in: *Supermolecular Dye Chemistry*, Springer, 2005, pp. 161–204.
- [42] Y. Zhu, H. Zeng, J. Xie, L. Ba, X. Gao, Z. Lu, Atomic force microscopy studies on DNA structural changes induced by vincristine sulfate and aspirin, *Microsc. Microanal.* 10 (2004) 286–290.
- [43] G. Tyagi, D.K. Jangir, P. Singh, R. Mehrotra, DNA interaction studies of an anticancer plant alkaloid, vincristine, using Fourier transform infrared spectroscopy, *DNA Cell Biol.* 29 (2010) 693–699.
- [44] E. Froehlich, A. Gupta, J. Provencher-Mandeville, E. Asselin, J. Bariyanga, G. Berube, H.A. Tajmir-Riahi, Study of DNA interactions with steroidal and nonsteroidal estrogen-platinum (II)-based anticancer drugs, *DNA Cell Biol.* 28 (2009) 31–39.
- [45] R. Marty, A.A. Ouameur, J.F. Neault, S. Nafisi, H.A. Tajmir-Riahi, AZT-DNA interaction, *DNA Cell Biol.* 23 (2004) 135–140.
- [46] D.K. Jangir, S. Charak, R. Mehrotra, S. Kundu, FTIR and circular dichroism spectroscopic study of interaction of 5-fluorouracil with DNA, *J. Photochem. Photobiol., B* 105 (2011) 143–148.
- [47] J.H. Choi, A.S. Banks, J.L. Estall, S. Kajimura, P. Bostrom, D. Laznik, J.L. Ruas, M.J. Chalmers, T.M. Kamenecka, M. Bluhner, P.R. Griffin, B.M. Spiegelman, Anti-diabetic drugs inhibit obesity-linked phosphorylation of PPAR γ by Cdk5, *Nature* 466 (2010) 451–456.
- [48] D.K. Jangir, S.K. Dey, S. Kundu, R. Mehrotra, Assessment of amsacrine binding

- with DNA using UV-visible, circular dichroism and Raman spectroscopic techniques, *J. Photochem. Photobiol.*, B 114 (2012) 38–43.
- [49] P. Kolodziejczyk, A. Garnier-Suillerot, Circular dichroism study of the interaction of mitoxantrone, ametantrone and their Pd(II) complexes with deoxyribonucleic acid, *Biochim. Biophys. Acta* 926 (1987) 249–257.
- [50] B. Rafique, A.M. Khalid, K. Akhtar, A. Jabbar, Interaction of anticancer drug methotrexate with DNA analyzed by electrochemical and spectroscopic methods, *Biosens. Bioelectron.* 44 (2013) 21–26.
- [51] C. Wan, X. Guo, F. Song, Z. Liu, S. Liu, Interactions of mitoxantrone with duplex and triplex DNA studied by electrospray ionization mass spectrometry, *Rapid Commun. Mass Spectrom.* 22 (2008) 4043–4048.
- [52] J.M. Fortune, N. Osheroff, Merbarone inhibits the catalytic activity of human topoisomerase II α by blocking DNA cleavage, *J. Biol. Chem.* 273 (1998) 17643–17650.
- [53] G.M. Morris, R. Huey, W. Lindstrom, M.F. Sanner, R.K. Belew, D.S. Goodsell, A.J. Olson, AutoDock4 and AutoDockTools4: automated docking with selective receptor flexibility, *J. Comput. Chem.* 30 (2009) 2785–2791.
- [54] P.A. Holt, J.B. Chaires, J.O. Trent, Molecular docking of intercalators and groove-binders to nucleic acids using Autodock and Surflex, *J. Chem. Inf. Model.* 48 (2008) 1602–1615.
- [55] C.G. Ricci, P.A. Netz, Docking studies on DNA-ligand interactions: building and application of a protocol to identify the binding mode, *J. Chem. Inf. Model.* 49 (2009) 1925–1935.
- [56] M. Shinomiya, W. Chu, R.G. Carlson, R.F. Weaver, F. Takusagawa, Structural, physical, and biological characteristics of RNA-DNA binding agent N8-actinomycin D, *Biochemistry* 34 (1995) 8481–8491.
- [57] A.D. Bochevarov, E. Harder, T.F. Hughes, J.R. Greenwood, D.A. Braden, D.M. Philipp, D. Rinaldo, M.D. Halls, J. Zhang, R.A. Friesner, Jaguar: a high-performance quantum chemistry software program with strengths in life and materials sciences, *Int. J. Quantum Chem.* 113 (2013) 2110–2142.
- [58] S. Saebø, W. Tong, P. Pulay, Efficient elimination of basis set superposition errors by the local correlation method: accurate ab initio studies of the water dimer, *J. Chem. Phys.* 98 (1993) 2170–2175.
- [59] S.F. Boys, F.d. Bernardi, The calculation of small molecular interactions by the differences of separate total energies. Some procedures with reduced errors, *Mol. Phys.* 19 (1970) 553–566.
- [60] L.A. Zwelling, J. Mayes, M. Hinds, D. Chan, E. Altschuler, B. Carroll, E. Parker, K. Deisseroth, A. Radcliffe, M. Seligman, et al., Cross-resistance of an amsacrine-resistant human leukemia line to topoisomerase II reactive DNA intercalating agents. Evidence for two topoisomerase II directed drug actions, *Biochemistry* 30 (1991) 4048–4055.
- [61] A. Skladanowski, S.Y. Plisov, J. Konopa, A.K. Larsen, Inhibition of DNA topoisomerase II by imidazoacridinones, new antineoplastic agents with strong activity against solid tumors, *Mol. Pharmacol.* 49 (1996) 772–780.
- [62] P. Vejpongsa, E.T. Yeh, Topoisomerase 2 β : a promising molecular target for primary prevention of anthracycline-induced cardiotoxicity, *Clin. Pharmacol. Ther.* 95 (2014) 45–52.
- [63] Y.-R. Wang, S.-F. Chen, C.-C. Wu, Y.-W. Liao, T.-S. Lin, K.-T. Liu, Y.-S. Chen, T.-K. Li, T.-C. Chien, N.-L. Chan, Producing irreversible topoisomerase II-mediated DNA breaks by site-specific Pt(II)-methionine coordination chemistry, *Nucleic Acids Res.* 45 (2017) 10861–10871.
- [64] J. Kluza, A. Lansiaux, N. Wattez, C. Mahieu, N. Osheroff, C. Bailly, Apoptotic response of HL-60 human leukemia cells to the antitumor drug TAS-103, *Cancer Res.* 60 (2000) 4077–4084.
- [65] L.J. Lewis, P. Mistry, P.A. Charlton, H. Thomas, H.M. Coley, Mode of action of the novel phenazine anticancer agents XR11576 and XR5944, *Anti Cancer Drugs* 18 (2007) 139–148.
- [66] W.M. Bonner, C.E. Redon, J.S. Dickey, A.J. Nakamura, O.A. Sedelnikova, S. Solier, Y. Pommier, GammaH2AX and cancer, *Nat. Rev. Cancer* 8 (2008) 957–967.
- [67] A. Ivashkevich, C.E. Redon, A.J. Nakamura, R.F. Martin, O.A. Martin, Use of the gamma-H2AX assay to monitor DNA damage and repair in translational cancer research, *Cancer Lett.* 327 (2012) 123–133.
- [68] E.P. Rogakou, W. Nieves-Neira, C. Boon, Y. Pommier, W.M. Bonner, Initiation of DNA fragmentation during apoptosis induces phosphorylation of H2AX histone at serine 139, *J. Biol. Chem.* 275 (2000) 9390–9395.
- [69] C.D. Kanakis, P.A. Tarantilis, C. Pappas, J. Bariyanga, H.A. Tajmir-Riahi, M.G. Polissiou, An overview of structural features of DNA and RNA complexes with saffron compounds: models and antioxidant activity, *J. Photochem. Photobiol.*, B 95 (2009) 204–212.
- [70] H.M. Berman, J. Westbrook, Z. Feng, G. Gilliland, T.N. Bhat, H. Weissig, I.N. Shindyalov, P.E. Bourne, The protein Data Bank, *Nucleic Acids Res.* 28 (2000) 235–242.
- [71] R. Huey, G.M. Morris, A.J. Olson, D.S. Goodsell, A semiempirical free energy force field with charge-based desolvation, *J. Comput. Chem.* 28 (2007) 1145–1152.
- [72] J. Foster, F. Weinhold, Natural hybrid orbitals, *J. Am. Chem. Soc.* 102 (1980) 7211–7218.
- [73] J. Chocholoušová, V. Špirko, P. Hobza, First local minimum of the formic acid dimer exhibits simultaneously red-shifted O–H and improper blue-shifted C–H hydrogen bonds, *Phys. Chem. Chem. Phys.* 6 (2004) 37–41.
- [74] K. Bojanowski, S. Lelievre, J. Markovits, J. Couprie, A. Jacquemin-Sablon, A.K. Larsen, Suramin is an inhibitor of DNA topoisomerase II in vitro and in Chinese hamster fibrosarcoma cells, *Proc. Natl. Acad. Sci. U. S. A.* 89 (1992) 3025–3029.
- [75] R.R. Tice, E. Agurell, D. Anderson, B. Burlinson, A. Hartmann, H. Kobayashi, Y. Miyamae, E. Rojas, J.C. Ryu, Y.F. Sasaki, Single cell gel/comet assay: guidelines for in vitro and in vivo genetic toxicology testing, *Environ. Mol. Mutagen.* 35 (2000) 206–221.